

Design and Fabrication of a High-gain Microstrip-fed Yagi-Uda Antenna

MAHYAR MODARESI



KTH Electrical Engineering

Master's Degree Project
Stockholm, Sweden

IR-SB-EX-0516

Design and Fabrication of a High-gain Microstrip-fed Yagi-Uda Antenna

Mahyar Modaresi 780812-A177

Advisor: Björn Lindmark

S3 department
Royal Institute of technology(KTH)
Stockholm
Sweden

July 11, 2005

Abstract

In this report, Yagi-Uda antenna is analyzed and simulated by developing a Matlab program. The analysis of Yagi antenna has been based on considering a single mode cosine current distribution on all elements. The antenna is viewed as a special kind of center-driven dipole array in which all but the actual exciter element are short-circuited at the terminals. Currents are induced in the parasitic elements via the mutual impedances with the exciter, and radiation occurs as from a set of discrete sources. The mutual impedance matrix of the array is calculated using EMF method and integral equations for electric field. This analysis has led to a fast and efficient code to calculate Yagi parameters. The validity of the results is checked with a MoM solution from NEC2, where good agreement has been observed in terms of radiation pattern. Then the code has been used together with genetic algorithm in order to optimize Yagi-Uda antenna for gain maximization. A 31-element high gain Yagi with 19.2dB gain and the gain bandwidth of 8 percent is derived in one optimization. Also the Pareto fronts are plotted for Yagi antennas with different number of elements which shows the trade off between directivity and front to back lobe(F/B) ratio. The effect of genetic algorithm parameters are also studied on the convergence of the optimization. Finally, a high-gain Yagi with 8 elements is fabricated on a dielectric substrate. The measured gain for this antenna at 2.4GHz is 11.4dB and the measured radiation pattern and input impedance shows a good agreement with HFSS simulation.

Acknowledgment

I would like to greatly thank my supervisor Dr. Björn Lindmark for his kind support and remarkable advices in this project. It has been mainly his patience and valuable ideas that helped me to finish this work. I should also specially thank Dr. Lotfollah Shafai at the university of Manitoba for his encouragement of the work and his practical ideas for implementing the antenna. Also, many thanks to Kjell Norén who helped me in making a wire Yagi antenna at KTH and many thanks for the cooperation from Gävle university which provided us a network analyzer for impedance measurement. I should greatly thank Brad Tabachnick who did the far-field measurements at the antenna and microwave lab at the university of Manitoba and also I should specially thank Allen Symmons and Cory Smit at the ECE Machine shop at the university of Manitoba for their kind help in fabrication. Also, many thanks to the Agilent Technologies representatives at ANTEM 2005 conference who did a radiation pattern measurement at 2.4 GHz using their near-field measurement setup(StarLab). I should also thank all the friends from S3 department at KTH for creating a nice atmosphere for my work and also my friends in applied EM group at the university of Manitoba who supported my work with their valuable ideas.

Contents

1	Introduction	3
2	Simulation of the Yagi array using thin wire approximation	5
2.1	Calculation of mutual impedance between dipoles using Induced EMF method and Integral Equations	5
2.2	Calculation of currents on elements	9
2.3	Radiation pattern of the array: Super-position of the radiated field by array elements	10
3	Genetic algorithm optimization of Yagi antenna	14
3.1	Objective Functions and Fitness Scaling	15
3.2	Selection	17
3.3	Representing Antennas as Chromosomes	17
3.4	Genetic Operators	18
4	Results obtained from genetic optimization for directivity of Yagi antenna	23
4.1	Optimized length and spacing for a 31-element high gain Yagi	23
4.2	Gain bandwidth of the optimized Yagi	24
4.3	Principal plane patterns of the optimized Yagi in different frequencies	25
4.4	Maximum directivity and F/B ratio for Yagi with 3, 4, 5 and 6 elements	26
4.5	Effect of genetic algorithm parameters on optimization convergence	29
5	Fabrication of Yagi-Uda array on dielectric substrate	33
5.1	Design of a Printed dipole with integrated Balun	34
5.2	Simulated and measured radiation patterns for a Yagi array on dielectric substrate	36
5.3	Impedance measurement	44
6	Conclusion and future work	46

Chapter 1

Introduction

In 1927 and 1928, respectively, Uda and Yagi published their papers on what today is known as the Yagi-Uda antenna [1],[2]. The Yagi-Uda antennas are the most common and known type of travelling wave antennas and since their discovery, they have received exhaustive analytical and experimental investigations in the literature. The simplicity of this antenna, together with its features has made it a proper choice for both amateur and professional antenna applications. This antenna has found applications from short waves to microwave frequencies.

The Yagi-Uda array can be described as a structure supporting a travelling wave. This surface travelling wave is described by the current distribution in each element and by the phase velocity of the travelling wave which means that these arrays can act as a wave guide under certain conditions. A thorough theoretical investigation in this sense has been done in [3] and [4].

A simple approach to calculate current distribution on Yagi elements is given by Green [5] which considers the Yagi-Uda antenna as a special kind of center-driven dipole array in which all but the actual exciter element are short-circuited at the terminals. Currents are induced in the parasitic elements via the mutual impedances with the exciter, and radiation occurs as from a set of discrete sources. Green has analyzed arrays with up to ten elements using this method with good results. An important consideration in this method is modelling the current distribution on the Yagi elements.

In the case of linear elements, such as those in Fig. 1.1, it has been found that an efficient representation for the current on element p is

$$I_p(z) = \sum_{n=1}^N I_{n_p} \cos(2n-1) \frac{\pi z}{L_p} \quad (1.1)$$

Where L_p is the length of the dipole. This series of odd-ordered even modes is chosen such that the current goes to zero at the ends of element p . This is a suitable approximation for elements whose diameter is small in terms of the

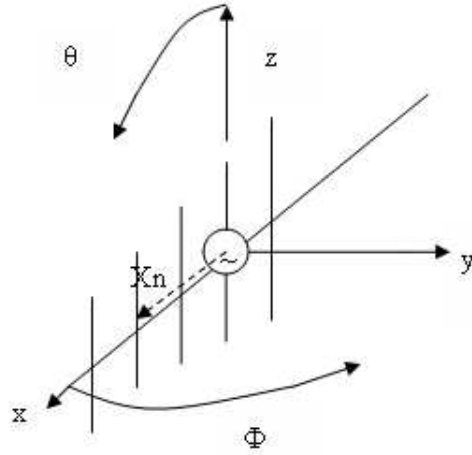


Figure 1.1: Coordinate system used to analyze Yagi-Uda array.

wave-length. Using more terms for current representation in (1.1) adds to the accuracy of the results but considering several terms in the series also increases the computational load of the analysis. It has been found that simulation time becomes the limiting factor in optimizing the Yagi antenna, specially when the number of elements becomes large. The approach taken in this report is based on the same method given by Green [5] and considering only the first mode cosine current distribution in (1.1) for all elements of the Yagi array.

Considering single-mode cosine current distribution, the mutual impedance between the elements is calculated using *Induced EMF* method. The currents on elements is then calculated by multiplication of the inverse of the mutual impedance matrix with the excitation vector which is an all-zero vector except for a one-volt excitation applied to the feed element.

Chapter 2

Simulation of the Yagi array using thin wire approximation

In this chapter the analysis method that is used in the report is explained. First the calculation of mutual impedance between dipoles using Induced EMF method is explained. After that, calculation of currents is discussed and then the radiation patterns are derived. The results are also verified by NEC2 software in this chapter.

2.1 Calculation of mutual impedance between dipoles using Induced EMF method and Integral Equations

The Induced EMF method was introduced by Brillouin in 1922 [6]. He used this method to calculate the self-impedance of small antennas, i.e., a loop and a dipole with uniform current distribution. The name "induced EMF method" was given by Pistolkors in 1929 [7]. Derivation given here is based on the conservation of complex power as described in [8].

Consider the two dipoles of Fig. 2.1, and imagine that they are enclosed in perfectly fitting surfaces, which include the sources. In that case there is neither power dissipation, nor energy storage in the volume surrounded by the surfaces; the dipoles are ideal conductors, and the generators take a very small volume. The power balance is reduced to

$$-\int \int_{gen.1,2} EK_e^* dS = \int \int_{1,2} (E \times H^*) \cdot \hat{n} dS \quad (2.1)$$

where K_e is the surface current and the asterisk denotes complex conjugate. This equation shows that the power delivered by the generators equals the surface integral of the Poynting vector. As the generators are very small, the left term of (2.1) may be written with voltages and currents. In the right term the H -field is related to the surface currents through the boundary conditions.

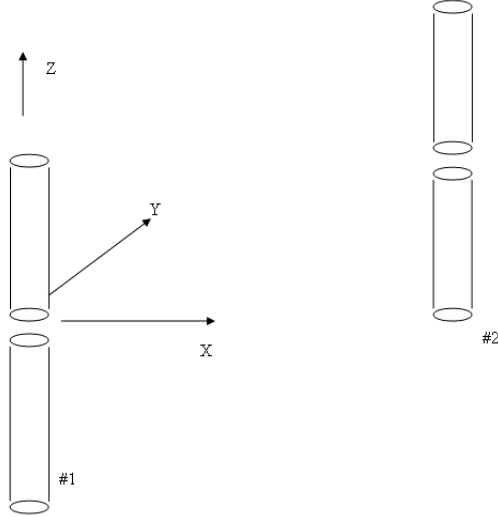


Figure 2.1: Two dipoles in free space.

Hence

$$V_1 I_1^* + V_2 I_2^* = - \int \int_{1,2} E K_e^* . dS \quad (2.2)$$

As the tangential field E , is zero on the surface of the dipole arms, the integral in (2.2) should extend only over the source region but according to [9,10,11] the integration should be carried out over the entire dipole surface when using approximate current distributions. There is no thorough theoretical evidence that leads to a generally valid conclusion but for the case of thin dipoles with assumed sinusoidal current distribution, it is well known that the integration has to be carried out over the entire surface.

We now return to (2.2) and proceed as follows. The voltage V_1 is written in terms of the elements of the Z -matrix

$$V_1 = Z_{11} I_1 + Z_{12} I_2$$

In the same way

$$V_2 = Z_{21} I_1 + Z_{22} I_2$$

The electric field in (2.2) is divided in four terms: E_{11} , E_{12} , E_{21} and E_{22} . The first index indicates the dipole at which surface the field point is situated,

the second indicates the dipole current which induces the field. Equation (2.2) can be written now as

$$\begin{aligned} Z_{11}|I_1|^2 + Z_{12}I_1^*I_2 + Z_{21}I_1I_2^* + Z_{22}|I_2|^2 = & - \int \int_{S_1} E_{11}K_{e1}^* dS_1 \\ & - \int \int_{S_1} E_{12}K_{e1}^* dS_1 - \int \int_{S_2} E_{21}K_{e2}^* dS_2 - \int \int_{S_2} E_{22}K_{e2}^* dS_2 \end{aligned} \quad (2.3)$$

where

E_{12} :The incident field at dipole 1 by current K_{e2}

K_{e1} :The electric current distribution on dipole 1

K_{e2} :The electric current distribution on dipole 2

I_1 :Total source current 1

I_2 :Total source current 2

Now put $I_2 = 0$, and assume that then $K_{e2} = 0$, i.e., no current is induced on dipole 2 by the current on dipole 1. (This means that the shape of K_{e2} is completely independent of K_{e1} . Its amplitude is set by I_2 , which in this case is also independent of I_1 because the excitation is with current sources having infinite internal impedance.) Now an expression for Z_{11} can be identified:

$$Z_{11} = \frac{-1}{|I_1|^2} \int \int_{S_1} E_{11}K_{e1}^* dS_1 \quad (2.4)$$

Likewise the expression for Z_{22} is found and by using the expression for Z_{11} and Z_{22} in (2.3) the expression derived for mutual impedance will be

$$Z_{12} = \frac{-1}{I_1^*I_2} \int \int_{S_1} E_{12}K_{e1}^* dS_1 \quad (2.5)$$

The equations (2.4) and (2.5) are based on the following assumptions:

- The current distributions are independent, in the sense that $K_{e1}(K_{e2})$ is fully determined by the value of $I_1(I_2)$.
- The dipole arms are perfect electrical conductors.
- The antennas are excited with surface currents that enclose a very small volume.
- The integration must be carried out over the entire current distribution, and not over the generator alone.

Equations (2.4) and (2.5) can be rewritten as follows:

$$Z_{11} = \frac{-1}{|I|^2} \int_{-l/2}^{l/2} E_{z11}I(z')dz' \quad (2.6)$$

$$Z_{12} = \frac{-1}{I_1I_2} \int_{-l_1/2}^{l_1/2} E_{z12}(z')I_1(z')dz' \quad (2.7)$$

Where l_1 is the length of the first dipole.

In order to calculate self and mutual impedances using (2.6) and (2.7), one need to calculate the near-field radiated electric field from a dipole with arbitrary length. Considering only the first term in (1.1) as an approximation for current distribution we will have

$$I(z) = I_0 \cos\left(\frac{\pi z}{L}\right) \quad (2.8)$$

An integral expression for the radiated electric field can be derived by this current as

$$E_z(x, y, z) = \frac{\lambda \sqrt{\mu/\epsilon}}{8\pi^2 j} I_0 \int_{-L_p/2}^{L_p/2} G(x, y, z|x', y', z') \cos\left(\frac{\pi z'}{L_p}\right) dz' \quad (2.9)$$

where

$$G(x, y, z|x', y', z') = \frac{\exp[-jkr]}{r^5} [(1 + jkr)(2r^2 - 3b^2) + k^2 b^2 r^2] \quad (2.10)$$

with

$$b^2 = r^2 - z^2 \quad (2.11)$$

and

$$r = \sqrt{(x' - x)^2 + (y' - y)^2 + (z' - z)^2} \quad (2.12)$$

A detailed derivation of this equation can be found in appendix A. The same expression is reported in reference [12].

An alternative current distribution that is used by some authors, as Balanis [21], is a piece-wise sinusoidal current given by:

$$I(z) = I_0 \sin[k(L/2 - z)]$$

for $0 \leq z \leq L/2$

$$I(z) = I_0 \sin[k(L/2 + z)]$$

for $-L/2 \leq z \leq 0$

This distribution is the same distribution for half wavelength dipoles as cosine distribution used in our report but it will be different for other length of dipoles. The piece-wise sinusoidal distribution introduces a discontinuity in current derivative at the center of the dipoles if the length is not equal to $\lambda/2$. This discontinuity is not realistic and leads to non-physical result.

By using piece-wise sinusoidal current in (A-8), the integral can be solved analytically. This closed form analytical solution is used in eq.(8-53) of Balanis [21] to calculate mutual impedance between dipoles.

In our work equation (2-9) is integrated numerically and then by using (2-9) in (2-6) and (2-7) the mutual and self impedance of dipoles with any length, distance and radius can be calculated. A *Matlab* code is developed to numerically integrate equation (2-6) and (2-7).

Figure 2.2 shows the mutual impedance between two half wavelength side by side dipoles with the radius equal to $10^{-5}\lambda$. The same graph can be found in figure 8.21a Balanis[21] where a piece-wise sinusoidal current is used.

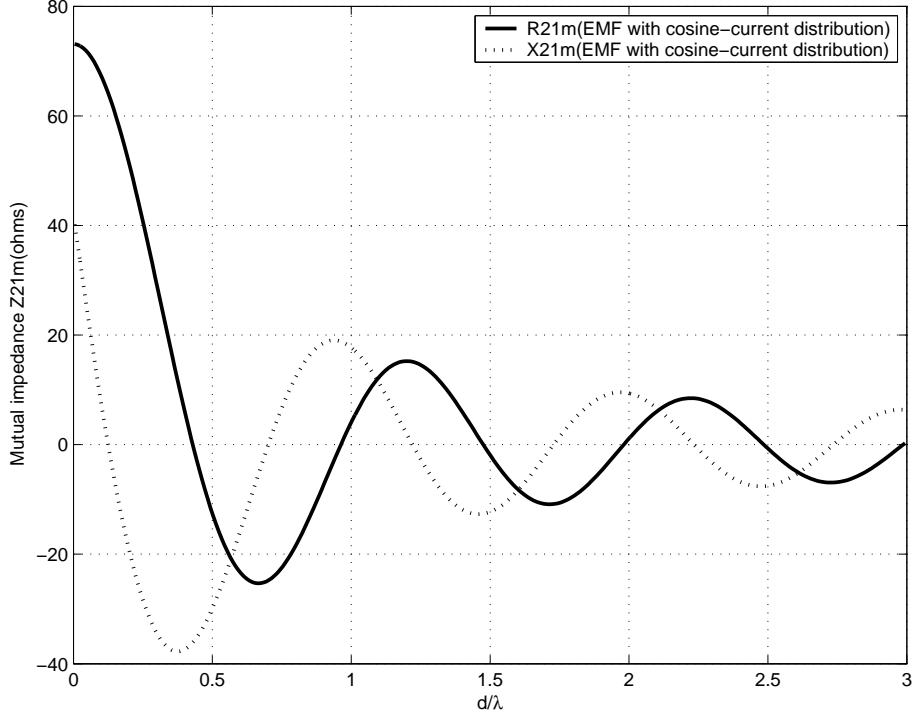


Figure 2.2: Mutual impedance of side-by-side half-wavelength dipoles with radius of $10^{-5}\lambda$

Calculating the self impedance using (2-6) needs some consideration as there is a singularity in the integrand due to the r factor in the denominator of the Green's function, eq. (2.10), which goes to infinity when calculating the self impedance of a dipole. However, having a nonzero dipole radius will help the integral to be solved but a finer division of integral path is needed. It is because of the fact that denominator of the integrand becomes very small and the integrand changes rapidly. In this case the convergence of the numerical integral should be checked to ensure getting the right answer for self impedance.

2.2 Calculation of currents on elements

Having the mutual impedance matrix of the array, the element currents can be easily calculated by considering a unity voltage source as the feed excitation applied to the center of the feed dipole. All other elements of the array can be considered to be short circuit and the currents can be calculated using the matrix relation $V = ZI$ which relates the current vector to the voltage vector of the array through the mutual impedance matrix. In this case the voltage vector would be equal to $V = [0, 1, 0, 0, 0, \dots]$ where all the elements are set equal to zero except the second element which represent the feed dipole voltage source.

Table 2.1 shows the spacing and length of a 4 element Yagi together with the corresponding element currents. The first row of currents shows the results from *Matlab* codes and the second row shows the results obtained from NEC2 code which is based on MoM method. Each element in MoM solution is divided into 6 pieces and designated currents in table 2.1 is the center current of each element which corresponds to the magnitude of the cosine form in our formulation(Refer to appendix C to see the commands used in NEC2 to model a Yagi antenna). It can be seen that there is a good agreement between two codes in the peak current on elements. All values in the table are shown with respect to the wavelength and the wire radius is equal to 0.00333λ in all the simulations in this report.

elem. no.	Reflector	Feed	Director 1	Director 2
length	0.4804	0.5	0.4553	0.4427
spacing	0.2624	-	0.1988	0.3412
Current(<i>Matlab</i>)	0.0076∠91.39	0.0175∠-79.47	0.0174∠107.21	0.0073∠-47.86
Current(<i>NEC2</i>)	0.0072∠90.12	0.0157E∠-81.91	0.0165∠103.49	0.0069∠-53.29

Table 2.1: Peak currents on the wires of a 4-element Yagi

2.3 Radiation pattern of the array: Superposition of the radiated field by array elements

The radiated electric field of an arbitrary length L dipole, having a current distribution given by (1.1) can be calculated from

$$E_{\theta} = j\eta \frac{I_0 \exp(-jkr)}{2\pi r} \frac{\pi k}{L} \frac{\cos(\frac{kL}{2} \cos \theta)}{(\pi/L)^2 - k^2 \cos^2(\theta)} \sin \theta \quad (2.13)$$

A detailed derivation of equation (2.13) can be found in appendix B.

Having the element currents and using (2.13), the far-field radiated electric field can be calculated for each element and the total radiation pattern is obtained by adding the contribution of each element.

Afterwards, radiation parameters of the antenna, namely directivity and side-lobe level, can be accurately extracted from radiation pattern provided that enough points were calculated in θ and ϕ directions.

The process that is used to obtain radiation patterns can be summarized as below:

1. The mutual impedance matrix of the array is calculated. In order to calculate the mutual impedance between dipoles one and two, equation

(2-9) is integrated numerically on the surface of dipole one to give the z-component of the electric field on the surface of the second dipole. Then, these values for z-component of electric field is used in equation (2-7) to give the mutual impedance. Equation (2-7) has been integrated numerically again.

2. After calculation of the mutual impedance matrix the currents on elements are calculated using the matrix multiplication of $I = Z^{-1}V$ with $V = [0, 1, 0, 0, 0, \dots]^T$. It means that all the dipoles are short-circuited except the feed dipole which is excited with a one-volt voltage source.
3. After having the current on all elements, equation (2-13) is used to calculate the radiation pattern of each dipole. Then this pattern is multiplied with a phase factor which comes from the distance of the dipole from the origin. Then the total pattern of the array is calculated by adding the patterns of all elements. Referring to figure 1.1, we can write the total electric field as

$$E_{total} = \sum_n I_n E_\theta(L_n) \cdot e^{jkx_n \cos \gamma}$$

with

$$\cos \gamma = \sin(\theta) \cos(\phi)$$

4. The directivity of the pattern is calculated using

$$D = \frac{4\pi |E_{tot}(\theta, \phi)|}{\int \int |E_{tot}|^2 d\Omega}$$

Electric field radiation pattern is calculated for all θ and ϕ angles with resolution of one degree and numerical integration is used to calculate the radiated power in the denominator of the directivity expression.

Figures 2.3 and 2.4 compare the calculated principal plane radiation patterns of the 4-element Yagi antenna, discussed in the previous section, with the results from NEC2. As it can be seen from the figures, the two codes agree well with each other in radiation pattern.

It can also be seen from figure 2.3 that for the E-plane radiation pattern, there is a discontinuity at $\theta = 90^\circ$ in simulations. This is due to the fact that the dipole radiation is zero along itself which can be seen from equation (2.13) with $\theta = 0$. This discontinuity is observed in all of the simulations for E-plane radiation pattern through the report.

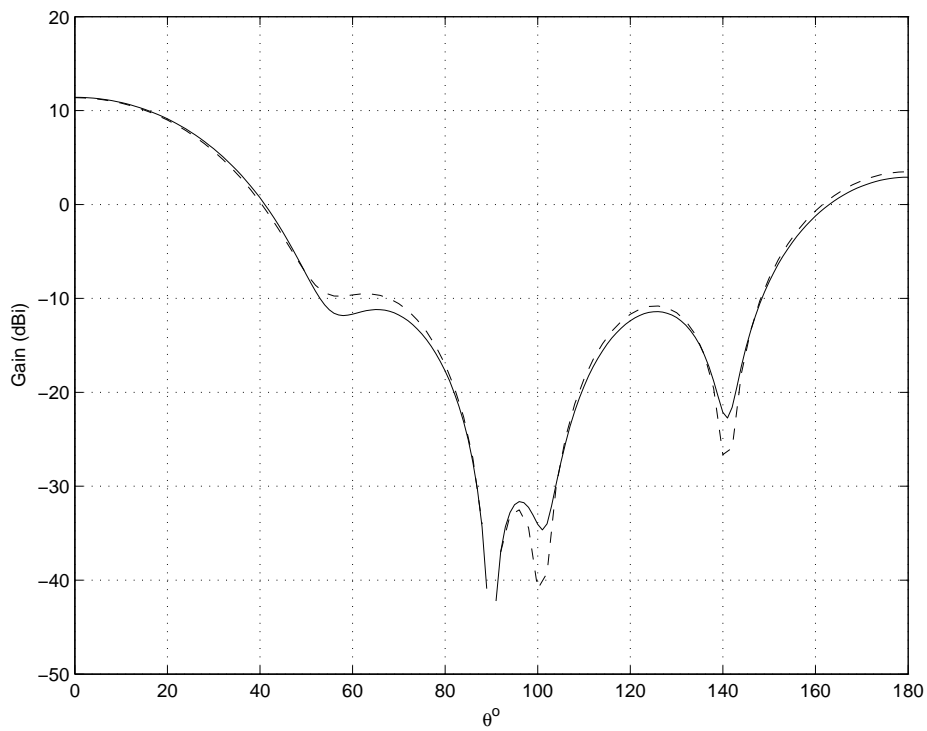


Figure 2.3: E-plane radiation pattern of the 4-element Yagi.(Solid line: Matlab result with $D(0)=11.41\text{dB}$, Dotted line:NEC2 result with $D(0)=11.37\text{dB}$)

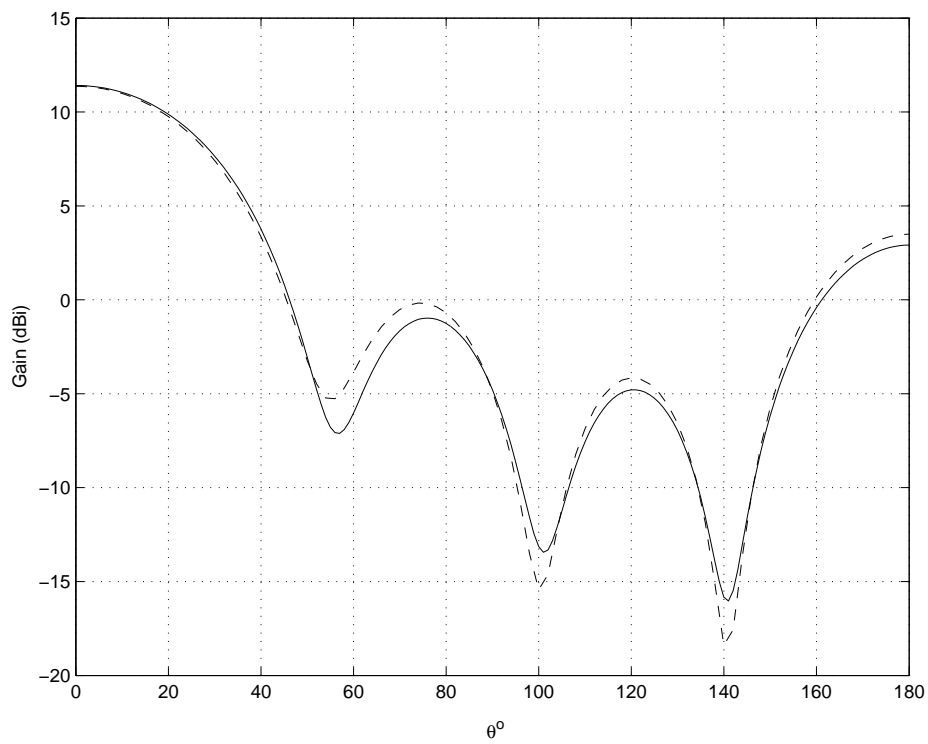


Figure 2.4: H-plane radiation pattern of the 4-element Yagi. (Solid line: Matlab result with $D(0)=11.41\text{dB}$, Dotted line:NEC2 result with $D(0)=11.37\text{dB}$)

Chapter 3

Genetic algorithm optimization of Yagi antenna

For optimization of Yagi antenna one can use either gradient-based or stochastic methods. Cheng has approached the Yagi optimization problem using a gradient-based method[13]. In our work, a genetic algorithm is used to optimize the element spacing and length of Yagi-Uda antenna. The evaluation of each of the antenna designs generated by the genetic algorithm (GA) during the optimization is done using the method described in previous sections. In this method only the first mode for element currents in (1.1) is considered which makes antenna evaluation faster than typical MoM based analysis. It was also shown in previous sections that the results of this method are accurate enough for radiation pattern optimization. Specially, Yagi-Uda antennas with large number of elements can be optimized rapidly.

In the following chapters, the length and spacing of Yagi-Uda antenna are optimized mainly for gain maximization. A brief introduction on genetic algorithm and its fundamental characteristics is given here.

Genetic algorithm is one of the stochastic optimization techniques that use the concepts of natural selection and genetics to conduct a global search of a solution space. The goal of the search is to find a good solution to the given problem.

There has been much interest in applying GAs and other stochastic optimization algorithms to the problem of Yagi-Uda optimization [14-19]. Simulation time is a key factor in using any optimization algorithm. In all these works, different versions of NEC code, a MoM-based software, has been used to evaluate each antenna design generated by the genetic algorithm.

In contrast to the MoM solution, the method discussed in earlier sections uses only one unknown coefficient for each element which will reduce the size

of the coefficient matrix to be equal to the number of elements. This will lead to a faster simulation of Yagi antenna.

Figure 3.1 shows a flow diagram of the GA used in the following chapter optimizations. Most of the steps shown are common to any genetic algorithm regardless of the problem being solved.

GAs begin a search with a large population of randomly generated individuals that are solutions to a problem. This randomness produces a diverse population of possible solutions representing a broad cross section of the entire solution space.

For the problem at hand, each individual in the population represents an antenna design. The characteristics of each design is evaluated and then assigned a fitness based on how closely the design meets the desired performance properties. By using a "survival of the fittest" paradigm, members of the population are selected to breed and have offspring. More fit individuals are assigned a larger probability of breeding. The idea is that by exchanging information between two good solutions, a better solution may be produced. There is also a small chance that an individual may mutate. This random altering of a small percentage of the population helps maintain the global nature of the search. New populations are produced and evaluated for many generations until the population converges to the same solution or some other stopping criteria are met.

3.1 Objective Functions and Fitness Scaling

The goal of the design process is to develop an antenna that meets or exceeds some desired performance characteristics. A few of the characteristics that define the antenna performance are side-lobe level, beam-width, bandwidth, front-to-back ratio, size, gain and input impedance.

The quality of a design is expressed mathematically by an objective function.

The following objective function, for example, rewards an antenna design x for having a high gain G and penalizes the design if the real part of the input impedance does not equal 50Ω or if the imaginary part of the input impedance Z does not equal zero.

$$o(x) = aG(x) - b|50 - \text{Re}(Z(x))| - c|\text{Im}(Z(x))| \quad (3.1)$$

The constants a, b and c are weights that control the contribution from each term to the overall objective function.

The fitness value used to rank the individual designs for the selection process is a scaled version of the objective function. Scaling the objective function serves two main purposes.

First, the selection phase requires that the fitness of an individual is a non-negative value while the objective function for many problems can become negative for some design parameters. Second, scaling is a useful way of controlling the competition between individuals. In early generations there is often a large discrepancy between the quality of the best and worst individuals in the population. This can lead to a situation where a single extremely fit individual begins to dominate the population, stifling the search for other good solutions, and resulting in premature convergence. By using a scaling function to reduce the difference in the fitness of individuals, population diversity is maintained. The exact opposite problem occurs in later generations when the population has begun to converge to similar solutions. Now the search is more localized because the population is full of similar, highly fit individuals. In this case, it is desirable to accentuate the differences between individuals so that the search is concentrated around the most promising solutions [20].

There are many approaches to scaling objective functions. One of the standard methods is linear scaling. Linear scaling translates objective functions to fitness values in the following manner:

$$f(x) = a.o(x) + b \quad (3.2)$$

The constants a and b are chosen so that an individual with the average objective value will have an average fitness value and so that fitness of the best individual is some desired multiple of the average fitness

$$f_{max} = C_{mult}f_{avg} \quad (3.3)$$

C_{mult} is usually between 1.2 and 2 for small populations of 50 to 100 individuals. The presence of negative objective scores complicates linear scaling. When negative values are present, it is not always possible to choose a and b in (3.2) such that (3.3) is satisfied and all individuals have positive fitness values [20].

Another approach to scaling objective functions, known as sigma truncation, is more appropriate in situations where negative objective scores are possible [20]. In sigma truncation scaling, the objective function is scaled according to

$$f(x) = o(x) - (o_{avg} - d.\sigma) \quad (3.4)$$

Here o_{avg} and σ are the average and the standard deviation of the objective function for the population. Extremely poor individuals with an objective value d standard deviations below the average end up with negative fitness

values. These individuals are assigned a fitness of zero. Reasonable values for d are between one and three [20]. The sigma truncation has been used in genetic optimization in the next chapters with $d = 2$.

3.2 Selection

After the population has been evaluated, individuals are selected from the population to contribute to the next generation. Some of the selected individuals are simply copied into the new population. Others are chosen to mate with another individual and their offspring become part of the new population. During selection, individual is assigned a probability of selection, based on the ratio of the individuals fitness to the total fitness of the member population

$$P_i = \frac{f_i}{\sum_{k=1}^N f_k} \quad (3.5)$$

and according to this probability each individual has a chance to be present in the next generation.

3.3 Representing Antennas as Chromosomes

Before discussing how individuals are combined through breeding to form new offspring, it is first necessary to see how an individual is represented in a GA. GAs work with chromosomes which are abstract representations of the solution to the problem. Thus, each individual solution in a population is represented by a chromosome.

As an example, a four-element Yagi-Uda array consists of a single driven element, one reflector element, and two director elements, is shown in Fig. 3.2.

This antenna array is described by specifying the length L of each element and the spacing S between adjacent elements.

One approach to represent the antenna as a chromosome is shown in Fig. 3.3. The parameters are discretized and encoded as binary values so that

$$L_{encoded} = l_1 l_2 \dots l_{B_L} \quad (3.6)$$

Here B_L is the number of bits used to represent L . B_L is found by

$$B_L = \lceil \log_2 \left(\frac{L_{max} - L_{min}}{L_{res}} + 1 \right) \rceil \quad (3.7)$$

where L_{min} and L_{max} define the range over which L can vary and L_{res} is the resolution of the discretization. If B_L is not an integer, it is rounded up to the next integer value. The binary representation of L is decoded by

$$L = L_{min} + \sum_{k=1}^{N_L} L_{res} l_k 2^{k-1} \quad (3.8)$$

The chromosome is formed by concatenating all the encoded parameters together into a single binary string. The size of the search space is defined by the length of the chromosome. As might be expected, GAs converge to a solution faster for smaller search spaces. Because of this, there is a tradeoff between the range and resolution allowed for the floating point parameters and the speed of convergence.

In all the optimizations in this report, 8 bits has been used to code each of the Yagi parameters. Although having a smaller resolution for parameters can lead to better solutions but choosing a very small resolution does not help in practice as there is always a limit for the accuracy of fabrication. So the best choice would probably be to take the resolution equal to the minimum accuracy in the fabrication process.

3.4 Genetic Operators

Information is propagated from one generation to the next using genetic operators. There are three basic genetic operators:

- Reproduction
- Crossover
- Mutation

Reproduction, the simplest of the operators, directly copies an individual from the old generation into the new generation.

The breeding of two chromosomes, accomplished using the crossover operator, is only slightly more complicated than reproduction. In crossover, information between two chromosomes is exchanged by cutting the chromosomes at a randomly chosen location and swapping the ends of the chromosomes to create two new chromosomes. Fig. 3.4 illustrates this process that provides a simple way for chromosomes to exchange information in a search for better chromosomes.

The percentage of individuals chosen to participate in crossover during each generation is specified by the parameter $p_{crossover}$ in the simulations. The value of 0.8 has been used for $p_{crossover}$ for the optimizations in this report. This means that 80 percent of the population are chosen randomly to go through this process and the rest 20 percent will be simply copied to the next generation without any change.

After several generations, it is likely that the population will contain multiple identical copies of a very fit individual. In general, this is desirable because the offspring from this individual are also likely to be fit; however, the offspring are also likely to be very similar to their parent which can lead to a localized search of the solution space. In order to maintain a more diverse population, the mutation operator is introduced. If a particular bit in a chromosome is chosen for mutation, the value of the bit is simply changed from zero to one or from one to zero.

By applying mutation to a small percentage of the population, the global nature of the search is preserved. The value of $P_{mutation} = 0.005$ has been used in most of the optimizations and in the last chapter the effect of $P_{mutation}$ is studied on the convergence of optimization.

The probabilistic nature of GAs results in a different solution for every run of the program, unless, of course, the problem is simple enough for the GA to find the optimal solution.

The GA also tends to find a "niche" solution and optimize it. For example, a fitness function for an antenna might include one term for maximizing gain and another to force the impedance toward 50Ω . If the best antennas from several different runs of the program are inspected, chances are that some of them will have good gain values with somewhat less desirable input impedance values, while others will have smaller gain values but better impedance values. Because of this, it is often useful to run the program several times and choose the antenna that best fits the application.

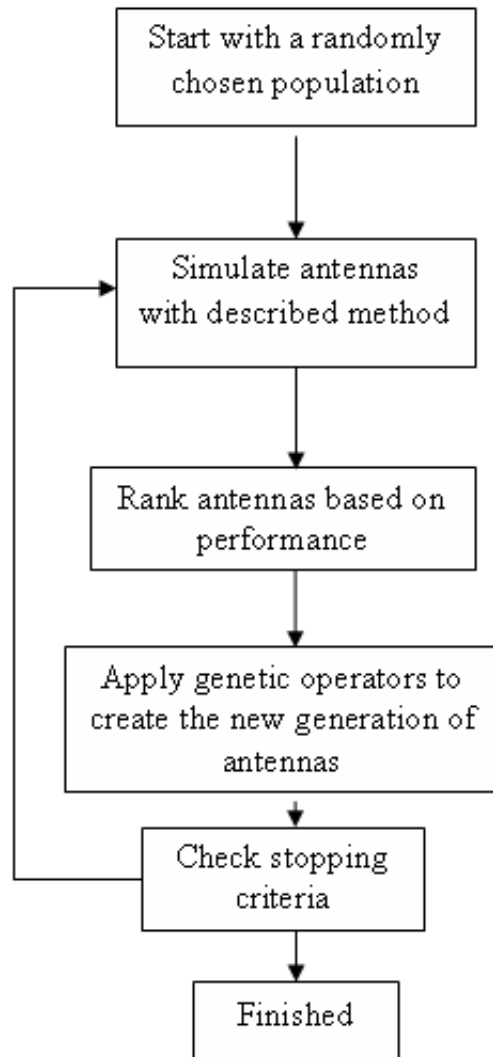


Figure 3.1: Flow diagram for the genetic algorithm used in Yagi-Uda optimization.

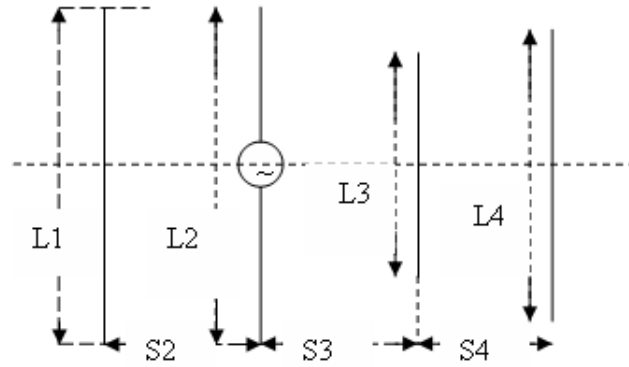


Figure 3.2: A thin wire antenna array with a single driven element, one reflector element, and two director elements.

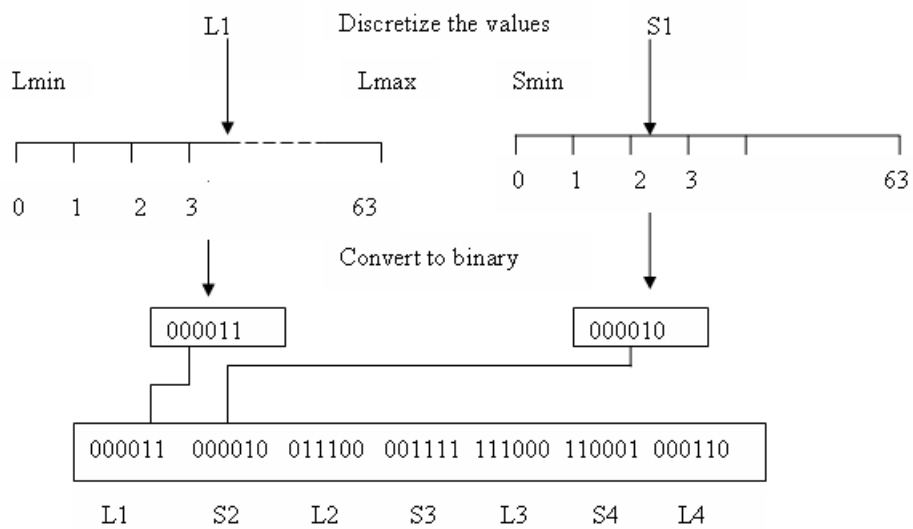


Figure 3.3: Each of the parameters in the problem are discretized, converted to binary values, and then concatenated together to form a single string. In this example, 6 bits were used to represent each value.

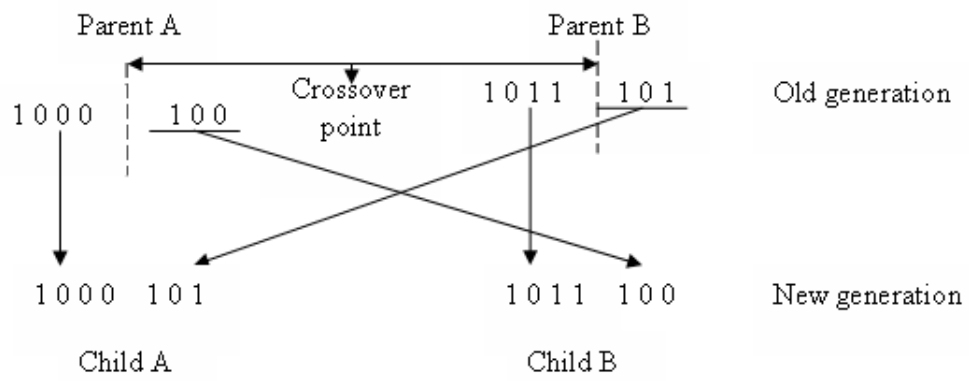


Figure 3.4: Two parent chromosomes from the old generation undergo crossover to produce two offspring in the new generation.

Chapter 4

Results obtained from genetic optimization for directivity of Yagi antenna

In this chapter the optimization results obtained from genetic algorithm for gain maximization of a Yagi antenna with 31 is given first. The gain has also been compared with the result from NEC2 software. Afterwards, the gain bandwidth of this antenna is studied followed by the plots of principal plane radiation patterns for different frequencies which shows a wide-band gain characteristic for Yagi antenna. After studying the characteristics of the 31-element high gain antenna, GA is used to maximize directivity of 3, 4, 5 and 6-element Yagi antennas and the effect of gain maximization is studied on F/B ratio by plotting Pareto fronts. The maximum gain obtained from G.A. is also compared with standard Yagi designs in this cases. In the last section of this chapter, the effect of GA parameters on the convergence of the algorithm are studied.

4.1 Optimized length and spacing for a 31-element high gain Yagi

A genetic optimizer has been run for a 31 element Yagi antenna to find the optimum length and spacing of the elements(except for the feed dipole length which is kept fixed and equal to $\lambda/2$).

One of the important issues in using genetic algorithm is to use appropriate values for algorithm parameters. In the study that has been done at the end of this chapter, it is found that choosing $P_{mutation} = 0.005$ gives the best performance of the algorithm when we choose $P_{crossover} = 0.8$. These values are used for all the optimizations in this report. The length of each element is chosen from the interval of 0.3λ to 0.7λ and the spacing between elements could vary from 0.1λ to 0.4λ in the optimization.

The number of individuals in each population was chosen to be 100 and the algorithm executed for 200 generations where not much improvement in gain was observed in the last generations.

In order to have a faster convergence, the fitness function used in optimization was the square of directivity in linear scale.

The results for the spacing and length of the elements are shown in table 4.1 for the best solution obtained from genetic algorithm. All data in table 4.1 are with respect to wavelength and the wire radius is equal to 0.00333λ .

The directivity of this design is equal to 19.1788 dB according to *Matlab* simulations while NEC2 shows the gain equal to 19.2dB which shows a good agreement between two codes in radiation pattern for long Yagi antennas as well. The NEC2 input file is given in appendix C.

elem. no.	Refl.	Feed	Dir.1	Dir.2	Dir.3	Dir.4	Dir.5	Dir.6	Dir.7
length	0.5024	0.5000	0.4584	0.4506	0.4318	0.3722	0.4255	0.3690	0.4161
spacing	0.2576	-	0.1624	0.2729	0.2741	0.1694	0.1329	0.3047	0.1353
elem. no.	Dir.8	Dir.9	Dir.10	Dir.11	Dir.12	Dir.13	Dir.14	Dir.15	Dir.16
length	0.4035	0.3925	0.4098	0.3878	0.4035	0.4098	0.3957	0.4114	0.4114
spacing	0.3188	0.1788	0.3847	0.3294	0.2118	0.2988	0.3047	0.3400	0.3965
elem. no.	Dir.17	Dir.18	Dir.19	Dir.20	Dir.21	Dir.22	Dir.23	Dir.24	Dir.25
length	0.3878	0.3878	0.3957	0.3643	0.3988	0.4161	0.3376	0.4082	0.3973
spacing	0.3529	0.2129	0.3976	0.2729	0.2553	0.3459	0.3929	0.3600	0.2647
element. no.	Dir.26	Dir.27	Dir.28	Dir.29					
length	0.3973	0.3910	0.3910	0.4271					
spacing	0.3529	0.3788	0.3706	0.3718					

Table 4.1: Optimized length and spacing for a high gain 31-element Yagi antenna with Directivity=19.1788 dB and F/B= 14.8858 dB.(Results are with respect to wavelength)

4.2 Gain bandwidth of the optimized Yagi

Gain versus frequency plot is shown in Fig. 4.1 for a 20 percent bandwidth for the antenna discussed in the previous section. As it can be seen from the graph, there is a slight drop in gain in the upper part of the center frequency compared to a sharp decrease in gain for the lower part of frequency band. It can also be seen that the total bandwidth in which the gain remains in the range of 3dB of the maximum gain is almost 8 percent of the center frequency which shows that this type of antennas are pretty wide-band in terms of gain.

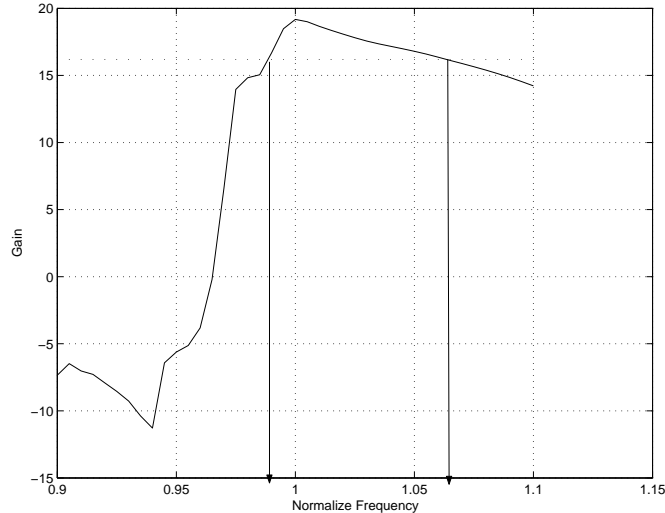


Figure 4.1: Frequency response for gain of the optimized Yagi in (2.1). Gain is calculated at $\theta = 90^\circ$ and $\phi = 0^\circ$

4.3 Principal plane patterns of the optimized Yagi in different frequencies

The E-plane and H-plane radiation power patterns of the Yagi antenna discussed earlier are plotted in Fig. 4.2 and 4.3 respectively for different frequencies. The solid line shows the results for center frequency and the dashed line and dotted lines are patterns for $0.98f_0$ and $1.02f_0$ respectively. It is assumed that Yagi elements are parallel to x -axis and lying along z -axis in the pattern plots.

As it can be seen from the patterns, there is a slight drop in gain for $f = 1.02f_0$, while there is almost 17dB improvement in the F/B ratio at this frequency and the side-lobes stay more or less in the same level as in the center frequency.

In contrast there is a large drop in gain at $f = 0.98f_0$ and the F/B ratio also deteriorate almost 9dB. There is also a significant increase in the side-lobe levels of the pattern.

One should not expect an excellent gain bandwidth for this design as the gain maximization in the center frequency has been the goal function for this optimized antenna. It is expected that better results can be obtained in terms of frequency response if the antenna is optimized for gain bandwidth goal function.

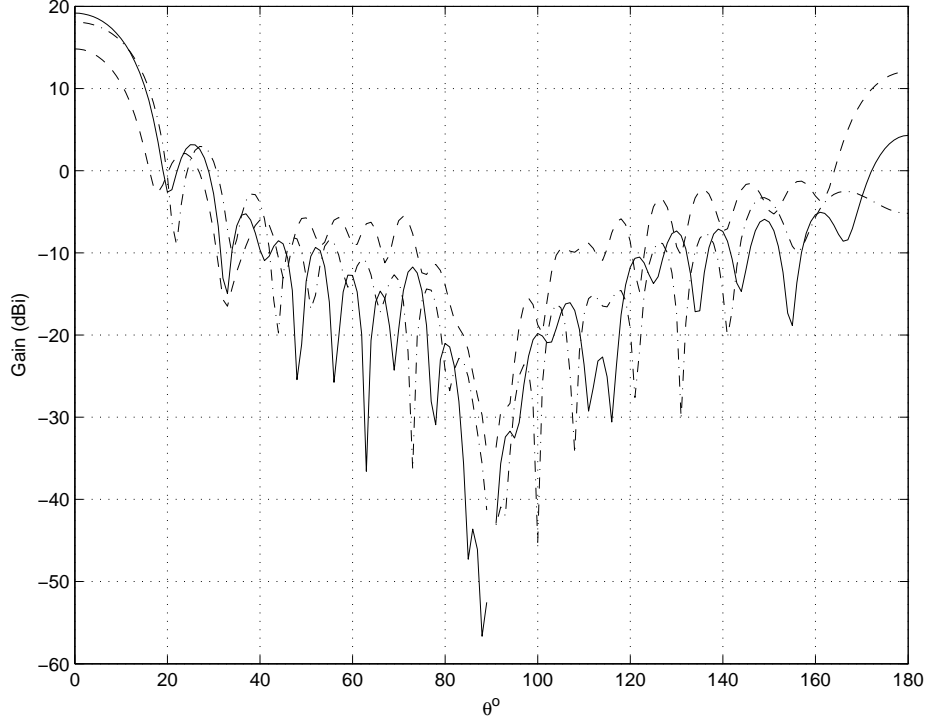


Figure 4.2: E-plane radiation pattern of optimized Yagi.(Solid line: f_0 , dashed line: $0.98f_0$, dashed-dotted line: $1.02f_0$)

4.4 Maximum directivity and F/B ratio for Yagi with 3, 4, 5 and 6 elements

In this section Yagi antennas with 3, 4, 5 and 6 number of elements are optimized for directivity. In each case the maximum directivity is compared with a standard Yagi from Table 10.6 of Balanis [21]. During the optimization for directivity, the values of F/B for each design are also saved in a vector and after the optimizations, they are plotted versus directivities by placing a dot in the graph for each design. Figure 4.4 shows this graph for 3-element Yagi antenna. By looking at this graph, one can see that there is no dot (design) beyond a curve which is shown in the figure as Pareto front. This curve is a front line that we can not have an antenna with more directivity and F/B beyond that and is called a Pareto Front.

The Pareto fronts are plotted to show the trade off between gain and F/B ratio. The graphs are generated from large populations obtained during the genetic optimizations where directivity and F/B ratio for all designs are saved during optimization but only the individuals having a higher gain than a threshold are selected to be included in Pareto fronts. This is done in order to see the Pareto fronts more clearly.

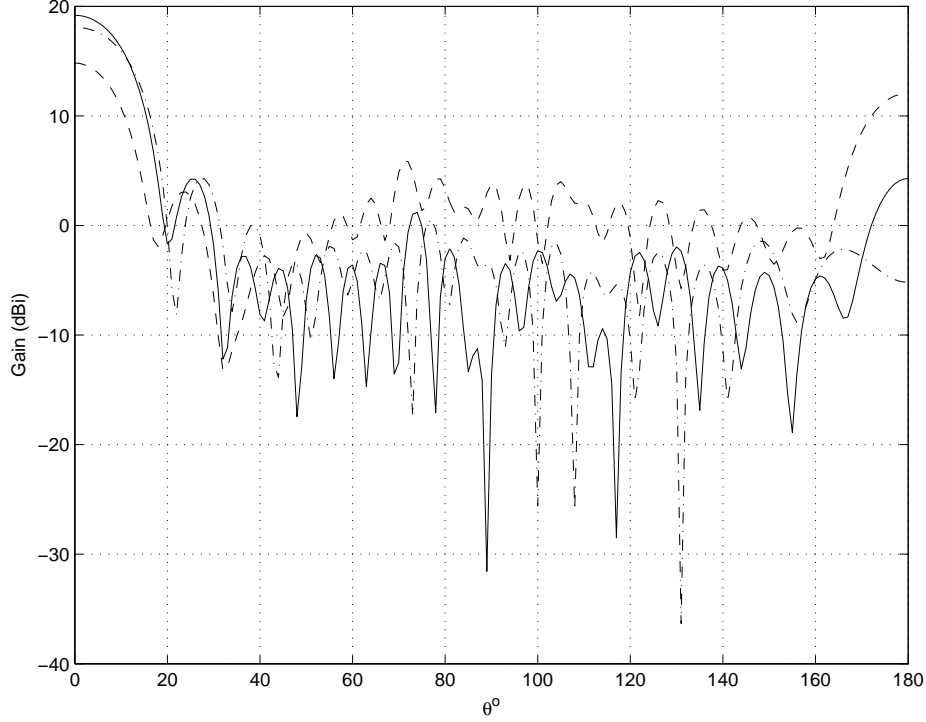


Figure 4.3: H-plane radiation pattern of optimized Yagi.(Solid line: f_0 , dashed line: $0.98f_0$, dashed-dotted line: $1.02f_0$)

For each of the graphs shown in (4.4) to (4.7), first the genetic algorithm has been run for maximizing solely for gain. The optimization is run for 60 generations for this goal. It is evident from the graphs that there are dense population of individuals in the high gain region which shows the population trend in the last generations of gain optimization. In order to see the Pareto fronts more clearly we need to have more points around the high gain region too. For this purpose, the last generation from gain optimization has been taken as a starting generation for a new optimization. This time the goal has been solely to maximize F/B ratio and the optimization has been run for 20 generation with this goal function. In other words, genetic algorithm is run for 80 generations. For the first 60 generations the goal function has been to maximize directivity. After finishing this optimization the population in the 60th generation (this population consists of 100 designs which all have very high directivities and are represented by the dots in the high-directivity and low-F/B part of the Pareto fronts) is taken as a starting population for the second optimization and this time F/B is optimized by running the GA for 20 generations. This will introduce some more random individuals around the high gain region and the Pareto fronts can be seen more clearly.

Finally, all the individuals that has occurred in the GA optimizations are plotted in the same graph to create the Pareto fronts shown in (4.4) to (4.7).

The plots are created for Yagi antennas with 3 to 6 number of elements and can give some idea as a design reference for the trade off between directivity and F/B.

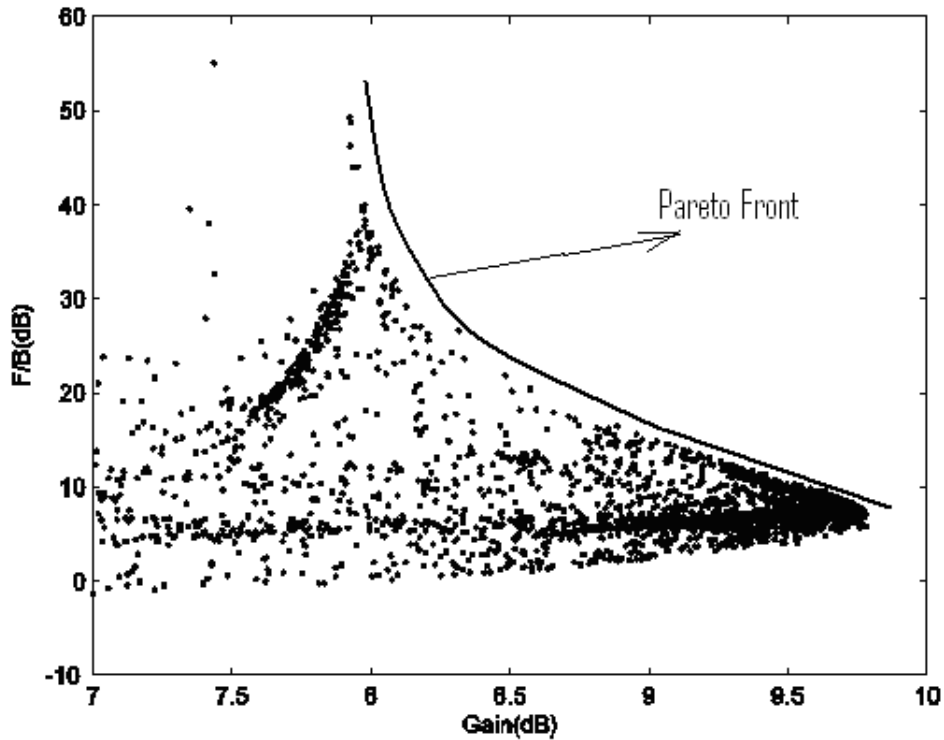


Figure 4.4: Pareto front for a 3-element Yagi antenna

It can be seen from the Pareto fronts that, in order to have a better F/B ratio one should sacrifice for the gain. This is a general concept in many disciplines where it is not possible to have a solution which is optimum for all the constraints.

To have a comparison of the directivities from Genetic algorithm with standard Yagi designs, the values of the maximum directivities for the optimized Yagi antennas in this section is compared with the standard Yagi designs reported in table 10.6 Balanis[21]. Maximum directivities for G.A optimized Yagi antennas can be found from figures 4.4 to 4.7. The comparison is shown in table 4.2.

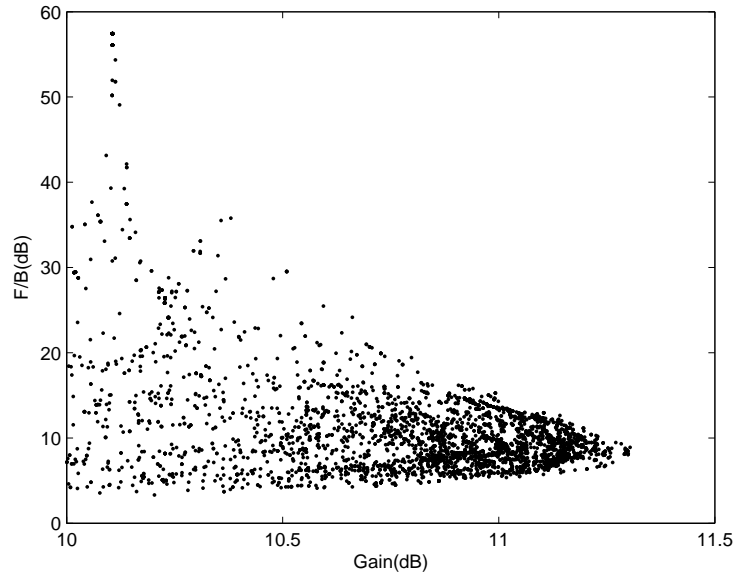


Figure 4.5: Pareto front for a 4-element Yagi antenna

Number of elements	3-element	4-element	5-element	6-element
Directivity from G.A.	9.8dB	11.3dB	11.48dB	13.57dB
Directivity of a standard Yagi	9.2dB	-	11.3dB	12.3dB

Table 4.2: Comparison of the G.A optimized Yagi antennas with standard Yagi antennas from Balanis

4.5 Effect of genetic algorithm parameters on optimization convergence

One of the important issues in using genetic algorithm is choosing appropriate values for its parameters. These parameters include: population size, crossover probability, mutation probability and number of bits to represent each individual. Proper choice of objective function and weighting coefficients, in case of optimizing for more than one goal, is also very important on how the algorithm behave. Algorithm will work well only if all of these values are chosen appropriately. If the parameters are not chosen correctly, genetic algorithm will not converge or it will converge to a local optimum point or convergence may take a long time.

There are some general guidelines in literature about choosing appropriate parameters for genetic algorithm. For example, many people choose mutation probability between 0.001 and 0.01 or population size is usually taken as 100 for optimization problems with small number of parameters and the crossover

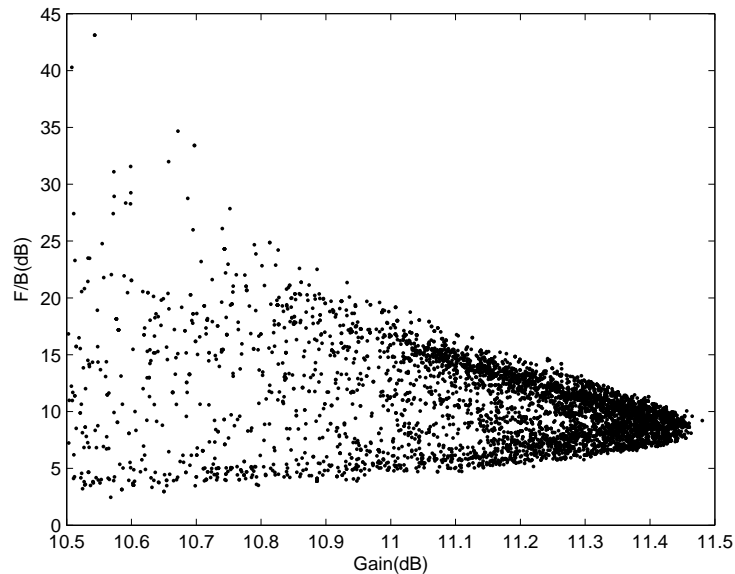


Figure 4.6: Pareto front for a 5-element Yagi antenna

probability is normally taken between 0.8 and 1. These values work for most of the optimization problems in the sense that they can guarantee a global search with fast convergence in most cases. However, each function is unique and has its special characteristic and behavior over its domain. This makes it necessary to use specific values for GA parameters for an optimum optimization. The best way to do this is testing different values for parameters and studying the behavior of the algorithm convergence in order to find out the appropriate parameters.

In this chapter the effect of choosing different values for $P_{mutation}$ has been studied for gain optimization of a 12 element Yagi antenna.

In figures 4.8 and 4.9 the maximum and the average gain of each generation are shown for different values of $P_{mutation}$ when the genetic algorithm has been run for gain maximization of a 12 element Yagi antenna. The $P_{crossover} = 0.8$ and graphs are plotted for $P_{mutation} = 0.01, 0.005$ and 0 . The maximum and average gain for each generation are in linear scale in the graphs. In all three cases algorithm has started from a random population in which the average gain is almost 0dB according the figure 4.9. Then it is observed that the average and maximum gain has increased in subsequent generations until the algorithm converges to a fit generation.

There is apparently a premature convergence for $P_{mutation} = 0$ to a local optimum point. As it can be seen from the figures the best and average gain

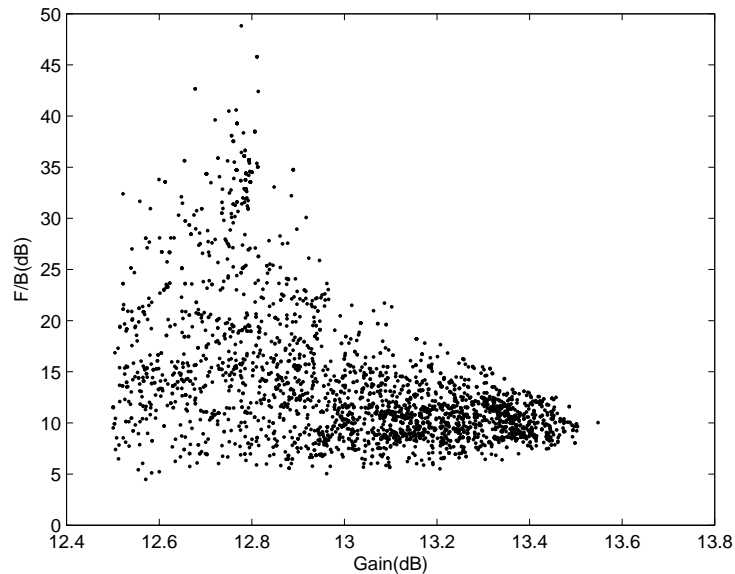


Figure 4.7: Pareto front for a 6-element Yagi antenna

stay constant in this case after 25th generation of algorithm. This means that all the members in the population has become the same and because there is no mutation, this design does not change and repeat itself in the next generations (Note that crossover of two identical chromosomes will lead to the same chromosome). On the other hand, as it can be seen the convergence has happened faster in this case but to a premature design!

These graphs clearly show the effect of mutation operation in the algorithm. By increasing $P_{mutation}$ to 0.005 the algorithm has converged to a better solution but the convergence is slower compared to $P_{mutation} = 0$. By increasing the $P_{mutation}$ further to 0.01, the convergence has become again slower compared to $P_{mutation} = 0.005$ as there is unnecessary up and down in the generations due to the random change of bits in mutation operation. This will increase the chance of finding the global optimum point but will reduce the convergence rate as well.

We have been able to find a good solution from $P_{mutation} = 0.005$ with a faster convergence compared to the other two values in this problem, so we conclude that $P_{mutation} = 0.005$ is the preferred values in the genetic optimization in this problem.

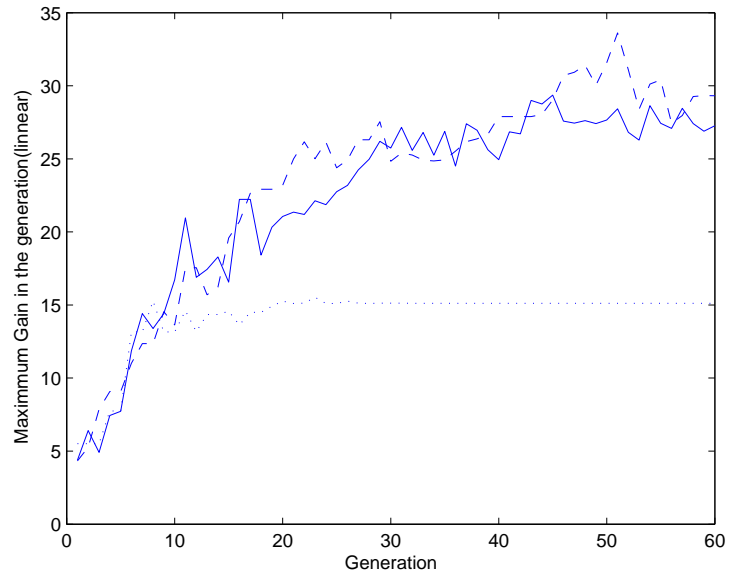


Figure 4.8: Plot of the best gain found in each generation (dotted line: $P_{mutation} = 0$, solid line: $P_{mutation} = 0.005$, dashed line: $P_{mutation} = 0.01$)

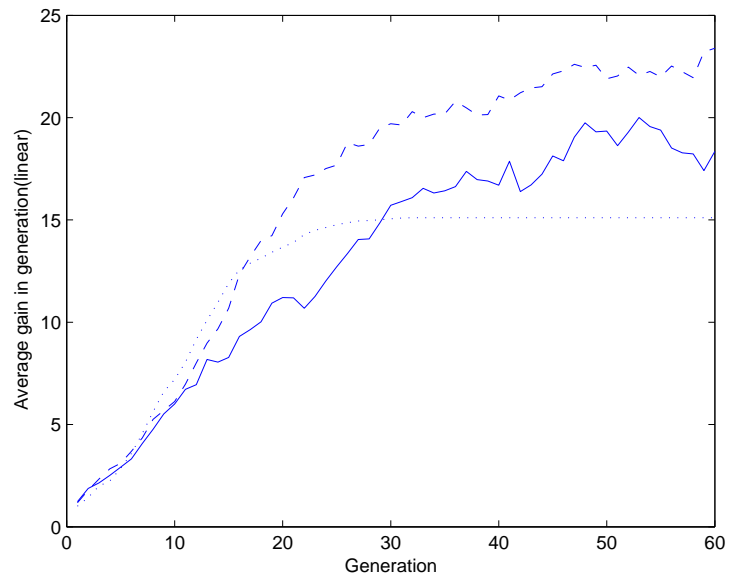


Figure 4.9: Plot of the average gain of all the individuals in each generation (dotted line: $P_{mutation} = 0$, solid line: $P_{mutation} = 0.005$, dashed line: $P_{mutation} = 0.01$)

Chapter 5

Fabrication of Yagi-Uda array on dielectric substrate

A microstrip line feed Yagi antenna will be discussed and the simulation results are compared with measurements.

Although analyzing Yagi-Uda antenna is pretty straight forward, there are several issues that should be considered in fabrication of this antenna. The most important issue is finding a way to properly feed the main dipole. The other thing is designing a structure that hold the parasitic elements. This holding structure should be designed in a way that does not perturb the normal operation of the Yagi antenna.

One possible way is to use a microstrip line and a microstrip line balun to feed the main dipole and using printed metallic strips on the same dielectric substrate as parasitic elements. The advantage of making Yagi antenna on a dielectric substrate is the possibility of the integration of the antenna with RF circuit since the RF circuitry use planar configuration too.

Designing a Yagi antenna on dielectric substrate has been of interest recently. Kaneda, Qian and Itoh have proposed a microstrip feed for a printed dipole[22]. This antenna system is actually a two-element Yagi with a plane acting as a reflecting element and the dipole being the feed element. Figure 5.1 shows this design. Grajek, Schoenlinner and Rebeiz have used the same feed structure to make a Yagi antenna at 24 GHz[23].

If the feed system in figure 5.1 is used, there will be some coupling effect between wire elements and ground plane and because of that it will not be possible to use the simple approach taken in this report to analyze Yagi antenna as our method is based on wire elements.

Instead of using the feed shown in figure 5.1 we have used a microstrip printed balun with a narrow ground plane to minimize the coupling between

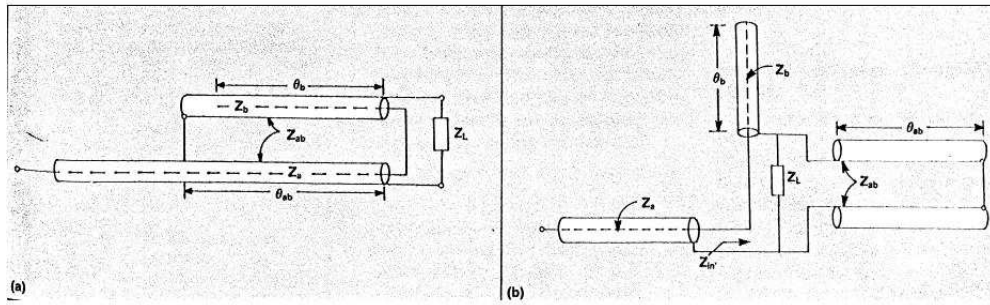


Figure 5.2: (a)Coaxial balun structure;(b)equivalent circuit[24]

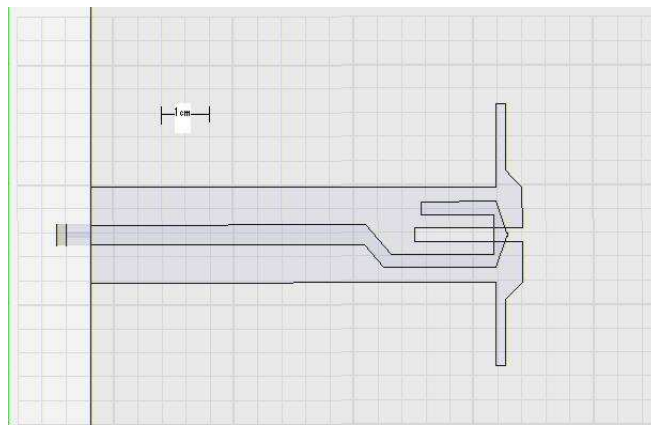


Figure 5.3: Printed circuit realization of balun structure with integrated dipole. The size of the background squares in figure are 0.5cm by 0.5cm.

The design in figure 5.3 has been made on a substrate with dielectric constant of 2.5 and thickness of 1.6mm and aimed to work at the center frequency of 2.4GHz.

The width of the microstrip line connected to the SMA connector is chosen to have 50Ω line impedance. The width of the ground plane is chosen to be small compared to the dipole length so it does not affect the radiation pattern of the dipole because of the coupling to the ground plane.

5.2 Simulated and measured radiation patterns for a Yagi array on dielectric substrate

In this part the radiation patterns of a high gain Yagi antenna with 8-elements is simulated and measured. The spacing and the length of this antenna is obtained from running a genetic optimizer with the same method that was discussed in previous chapters. Table 5.1 shows the dimensions of this optimized antenna.

elem. no.	Feed	Dir. 1	Dir. 2	Dir. 3	Dir. 4	Dir. 5	Dir. 6	Dir. 7
length	0.5	0.453	0.443	0.235	0.427	0.436	0.358	0.427
spacing	-	0.161	0.272	0.265	0.201	0.291	0.201	0.296

Table 5.1: Dimensions of a high gain 8-element Yagi without reflector (directivity=13dB). All values are with respect to the wavelength and wire-radius=0.004 λ

The array is optimized without having a reflector. Adding a reflector behind the main dipole will cause some complications in our design because of the coupling between reflector and feed line. Because of this the Yagi antenna has been optimized with only directors. The optimized 8-element antenna shown in table 5.1 has 13dB gain. One should note that the directivity of this optimized Yagi antenna (without reflector) is less than the maximum achievable directivity from a classical Yagi (Yagi with one reflector) with the same number of elements.

There are several practical issues that must be considered in fabrication of the Yagi antenna on dielectric substrate by using metallic strips.

First of all the numerical simulations we did for the Yagi antenna is for the antenna with cylindrical elements but the implemented parasitic elements are narrow stripes. C. M. Bulter has shown in [25] that the equivalent radius of a narrow conducting stripe is one-fourth of its width. This means that the width of the elements of the antenna in Table 5.1 should be made equal to 2 mm at 2.4 GHz operation of the antenna.

The second issue that must be taken into account when implementing the antenna is the end-cap effect. When the wire elements are built they behave as if they are a bit longer than their real length. As we will see later, it is found that the effective length of the elements is almost equal to the physical length plus the diameter of the elements.

The third issue and maybe the most important one is the effect of the dielectric substrate on the operation of Yagi antenna. In the numerical simulations

done for Yagi antenna we assumed that the elements are in free space but in reality they are placed on a substrate with dielectric constant of 2.5 which will have some effect on the operation of antenna.

P. R. Grajek, B. Schoenlinner and Gabriel M. Rebeiz, has reported this effect on their work in making a Yagi antenna on dielectric substrate. According to their work there will be a shift in operating frequency of the Yagi because of the added capacitance from supporting dielectric substrate. This effect can be compensated by a simple scaling of the antenna dimensions.

In order to find the frequency shift of the antenna due to the substrate effect in our design, the directivity is plotted for a range of frequencies in HFSS and the plot of directivity versus frequency obtained from HFSS is compared with the same plot obtained from the Matlab simulations. It was interesting to see that both of the graphs show the same pattern except for a shift in center frequency.

The procedure used to determine the scaling factor is as below. At first, the dimensions of the Yagi antenna has been calculated from the normalized values in table 5.1. With scaling these normalized values to 2.4Ghz, assuming the free space speed of light equal to $3 * 10^8 m/s$, the elements has been entered to the HFSS model by taking into account the end-cap effect. Then the HFSS simulation is run for a range of frequencies.

The directivity plots versus frequency showed the same pattern in two simulations (HFSS and Matlab) except for a shift in center frequency. Then the scaling factor needed to be implemented to the Yagi dimensions has been calculated by dividing these two frequencies.

It is turned out that this scaling factor for our design is equal to 0.844. In other word all the spacing and length of the elements in free space should be scaled with the factor of 0.844; We can thus assign an effective ϵ_{reff} to the substrate from the equation $1/\sqrt{\epsilon_{reff}} = 0.844$ which gives $\epsilon_{reff} = 1.4$. This is very close to the value reported in [23].

After considering the end-cap effect, elements can be built on the substrate.

Figure 5.4 and 5.5 shows the radiation pattern from HFSS simulation and EMF method. The graphs show the patterns from HFSS model with and without considering the end-cap effect. The patterns are plotted when the effect of end-cap has not been considered and when the length of the wires has been reduced by 1mm and 2mm to compensate for this effect. As it can be seen the best result is when the length of the wires are decreased by 1mm.(Note that the width of the wires is 2mm);

There is 2.6dB difference between the directivity given from the Matlab code and HFSS(Gain from Matlab is 13dBi and from HFSS is 10.4dBi) while the F/B lobe ratio match good for both cases. It is also interesting to note that the place of the side-lobes and nulls of pattern from HFSS and Matlab match pretty good for the case that we have not compensated for the end-cap effect($\delta l = 0$).

Having in mind that the width of the stripes is 2mm it means that the best results are obtained when we cut 0.5mm from each end of the wires. This is equal to the effective radius of the equivalent cylindrical wire according to[25].

The antenna has been made on a dielectric substrate with dielectric constant equal to 2.5 and the thickness of 1.6 mm . The metallic stripes are copper tapes which are cut with a cutter and a SMA connector has been soldered to the microstrip line as depicted in figure 5.6.

The measured radiation pattern of this antenna is plotted and compared with the results from HFSS simulation in figure 5.7 and 5.8.

The measured cross-polar components in E-plane and H-plane are also plotted in figures 5.7 and 5.8. As it can be seen the cross polar component is at least 20dB below the main lobe both in simulation and measurement.

The measurement has been done at the compact range anechoic chamber with 2 degrees resolution in two perpendicular planes. Figures 5.9 shows the antenna under test for H-plane measurement. As it can be seen from the figure 5.9, it has not been possible to measure the back-lobe of the antenna with this mounting system and the measurement has been done for only 180 degree rotation of the antenna(90 degrees rotation from end-fire direction in two directions).

Another measurement has been done in a Compact Laboratory for Spherical Near-Field Antenna Measurement (StarLab). Figure 5.10 shows the antenna under test and figure 5.11 and 5.12 show the E-plane and H-plane co-polar radiation patterns from the measurement and simulations.

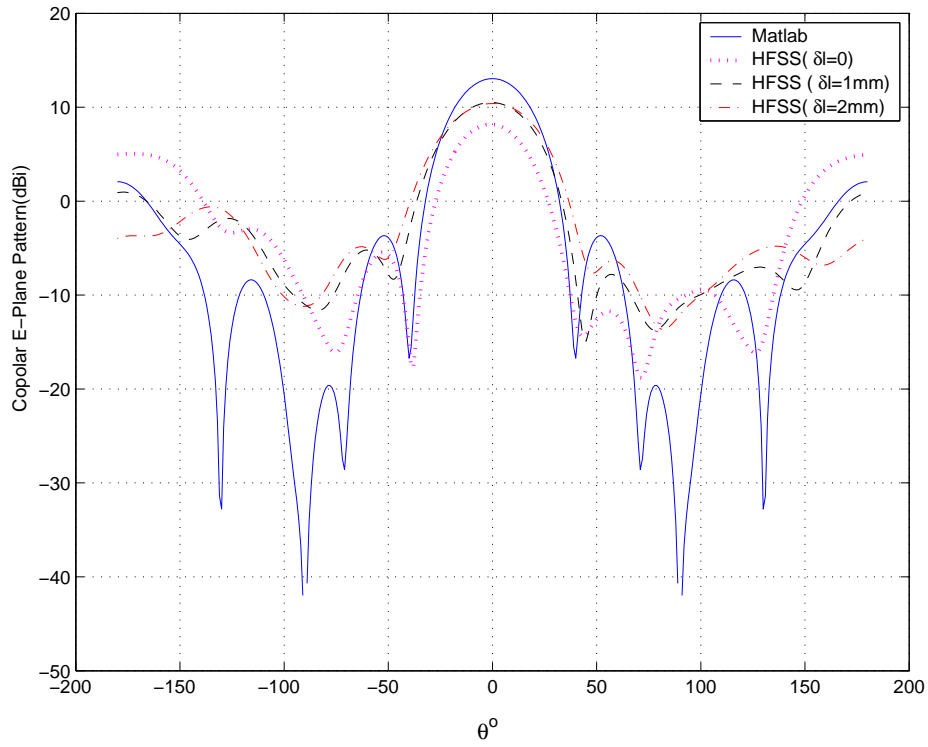


Figure 5.4: E-plane radiation pattern from EMF method and HFSS simulation for different effective length.

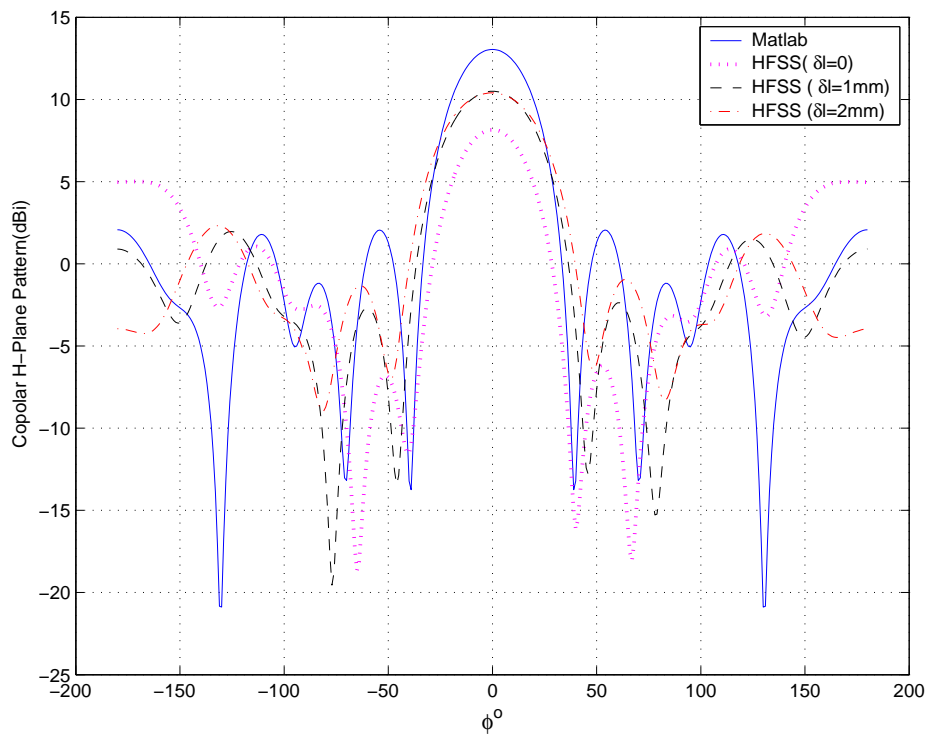


Figure 5.5: H-plane radiation pattern from EMF method and HFSS simulation for different effective length.

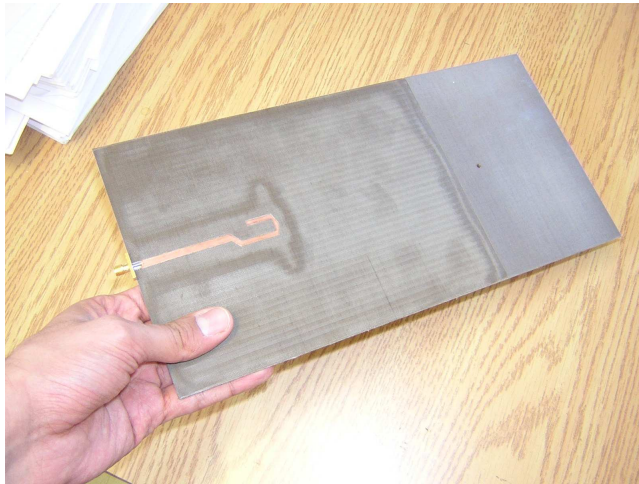
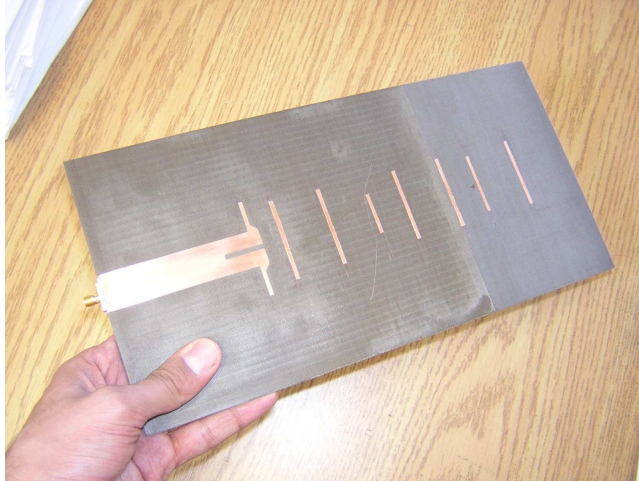


Figure 5.6: Fabricated antenna on dielectric substrate

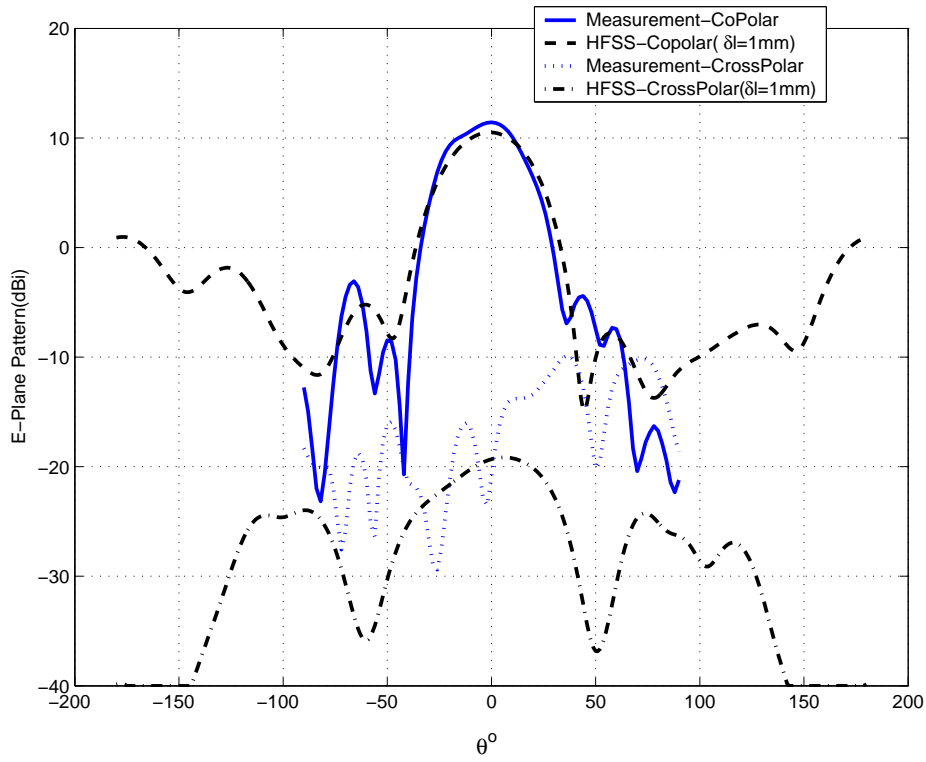


Figure 5.7: Measurement and HFSS E-plane radiation pattern.

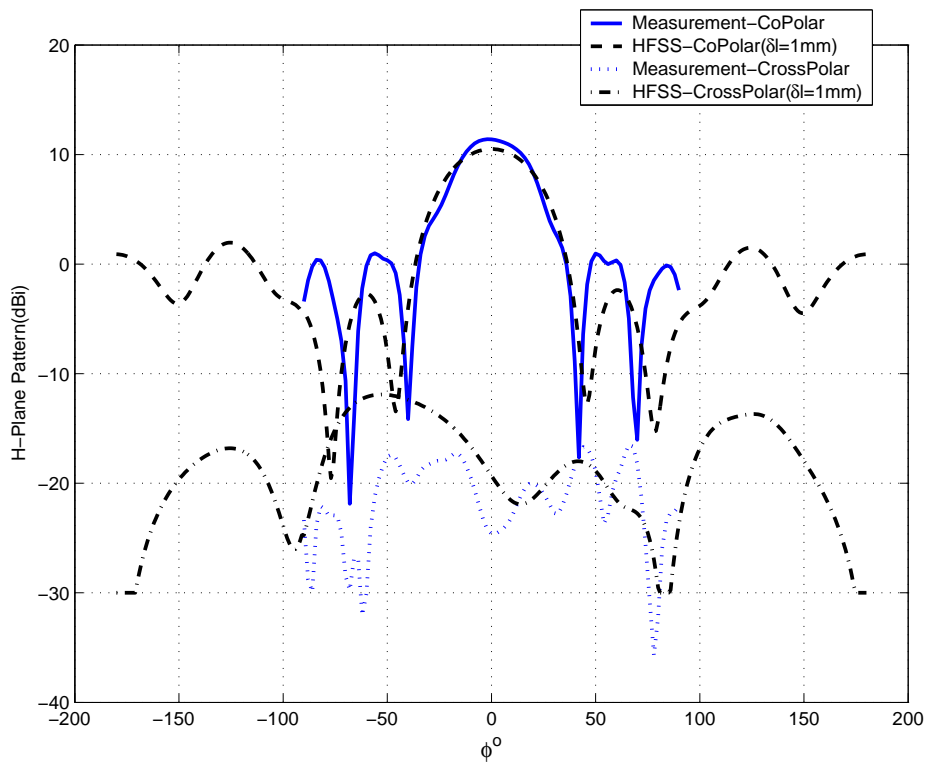


Figure 5.8: Measurement and HFSS H-plane radiation pattern.

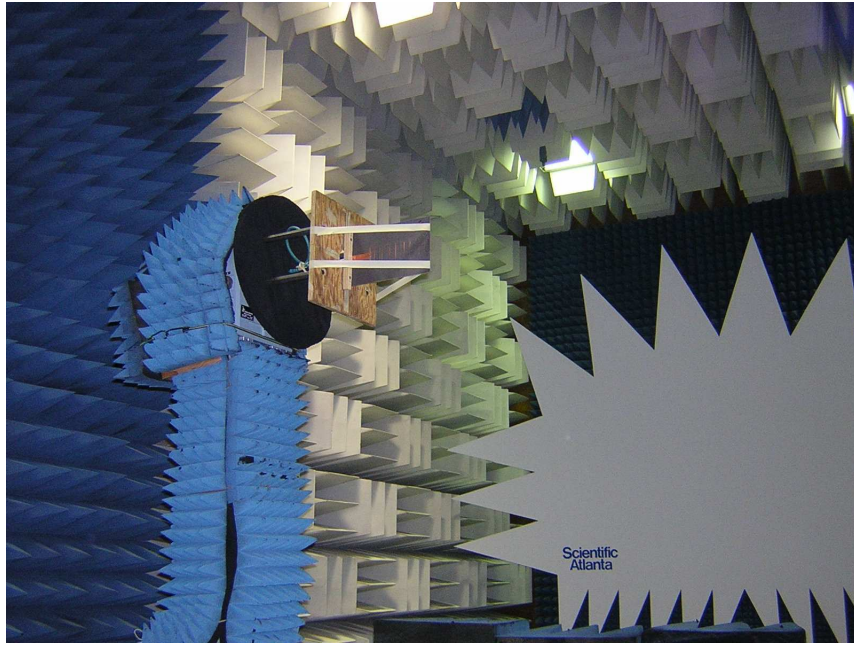


Figure 5.9: Antenna under test for H-plane radiation pattern(Compact range).



Figure 5.10: Antenna under test for radiation pattern measurement(StarLab).

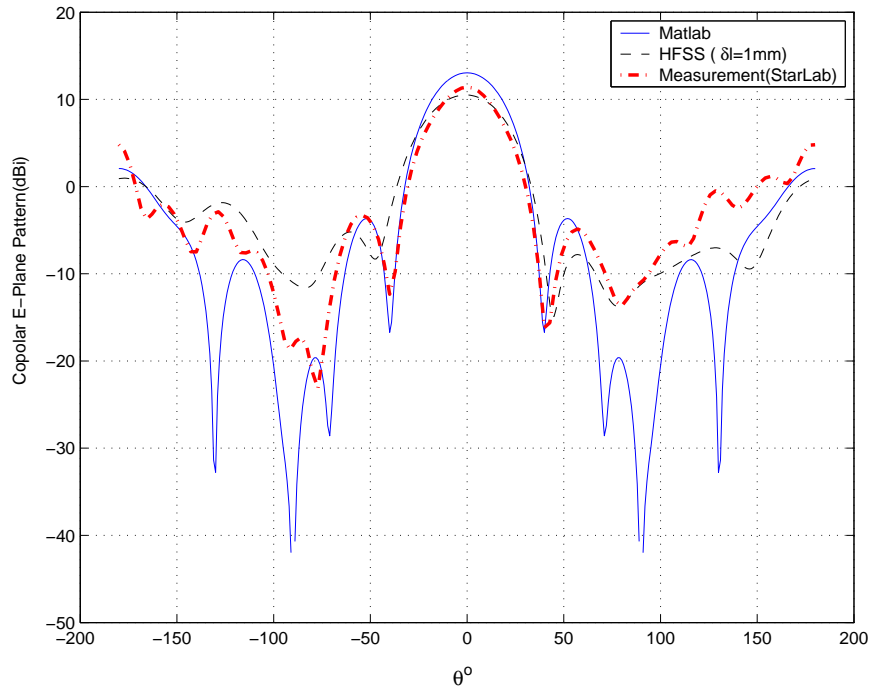


Figure 5.11: Measurement, Matlab simulation and HFSS E-plane radiation pattern. Directivity: Matlab:13dB, HFSS:10.4dB, Measurement(StarLab):11.4dB

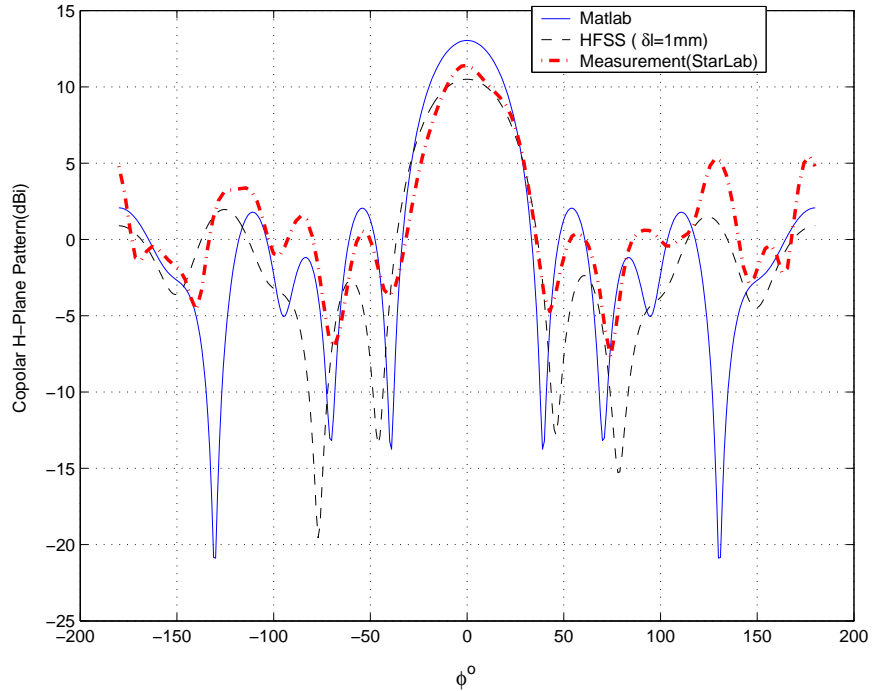


Figure 5.12: Measurement, Matlab simulation and HFSS H-plane radiation pattern. Directivity: Matlab:13dB, HFSS:10.4dB, Measurement(StarLab):11.4dB

5.3 Impedance measurement

Figure 5.13 shows the S11 plot of the Yagi array discussed earlier. As it can be seen there is a reasonable agreement between HFSS result and measurement.

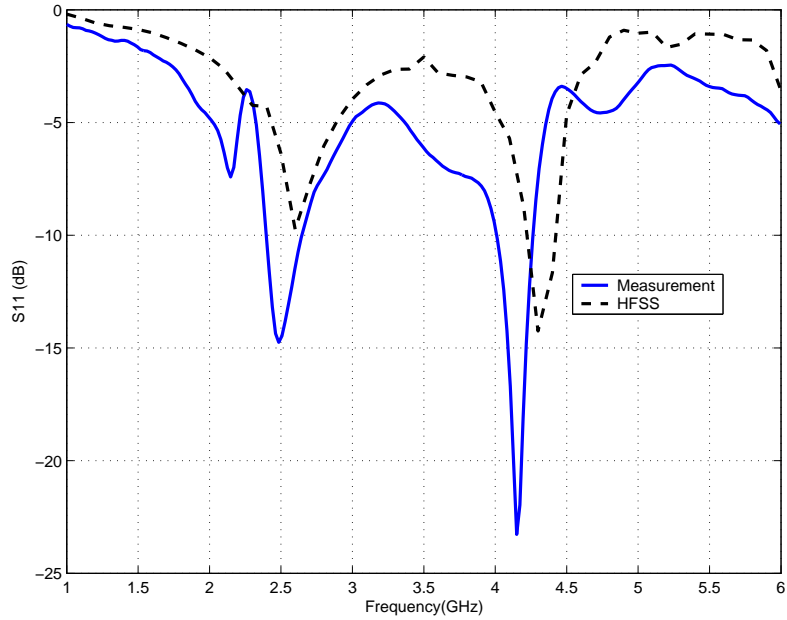


Figure 5.13: S11 plots.

Figure 5.14 shows the setup for impedance measurement.

There is a good matching in measurement at the center frequency of 2.4GHz with $S_{11} = -10\text{dB}$. In order to have a better matching we could use a $\lambda/4$ transformer or double stub matching to match the input impedance at 2.4GHz to the center of Smith chart.

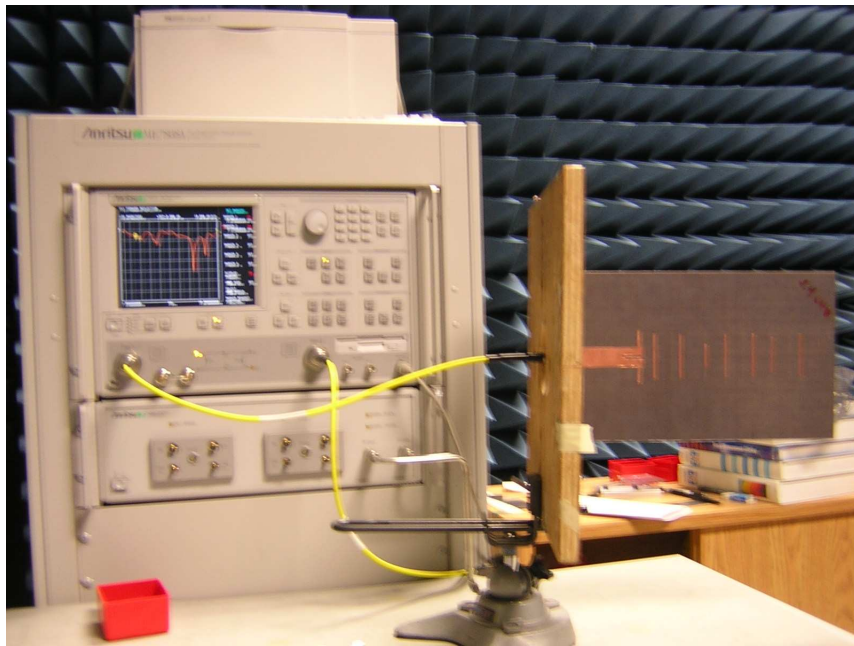


Figure 5.14: Antenna under test for impedance measurement.

Chapter 6

Conclusion and future work

The analysis of Yagi-Uda antenna, using a single mode cosine current distribution, has been studied in this report with using EMF method to calculate the mutual impedance matrix of the array. This method which is an efficient way to analyze Yagi antenna gives accurate results compared to a MoM-based(NEC2) code. It is also found that the Genetic algorithm is a suitable optimization tool for Yagi antenna and a high gain 31-element Yagi is obtained from this algorithm with 19.2dB gain. This gain-optimized antenna shows almost 8 percent gain bandwidth with a sharper drop in the lower part of frequency band. Pareto fronts were plotted for Yagi antennas with different number of elements. These graphs show a trade-off between gain and F/B ratio stating that there is no design with optimum gain and F/B ratio. The effect of $P_{mutation}$ was studied on the genetic algorithm convergence which shows the importance of choosing right parameters in the algorithm. Finally, the measurement results has shown that it is possible to make Yagi antenna on dielectric substrate with a microstrip feed.

This novel design can be adjusted to work in higher frequencies which makes it possible to add more directors and thus get higher gains. Another interesting issue is to add parasitic elements on the whole surface of the substrate which is the extension of Yagi antenna to two dimensions. This can increase the gain further by proper optimization of the parameters.

Bibliography

- [1] S. Uda, Wireless beam of short electric wave, J. IEE (Japan), pp. 273-282, March 1926, and pp. 1209-1219, November 1927.
- [2] H. Yagi, Beam transmission of ultra short waves, Proc. IRE, vol. 16, pp. 715-741, June 1928.
- [3] R. J. Mailloux, Antenna and wave theories of infinite yagi-uda arrays, IEEE Transactions on Antennas and Propagation, pages 499-506, July 1965.
- [4] R. J. Mailloux, Excitation of a surface wave along an infinite yagi-uda array, IEEE Transactions on Antennas and Propagation, pages 719-724, September 1965.
- [5] H. E. Green, Design data for short and medium length Yagi-Uda arrays, Elec. Engrg. Trans. Inst. Engrs. (Australia), pp. 1-8, March 1966.
- [6] L. Brillouin, Sur l'origine de la resistance de rayonnement, Radioelectricite, vol. 3, pp. 147-152, Apr. 1922.
- [7] A. A. Pistolokors, The radiation resistance of beam antennas, Proc. IRE, vol. 17, no. 3, pp. 562-519, Mar. 1929.
- [8] B.K.J.C Nauwealers and A.R.E De Capelle, Integrals for the Mutual Coupling Between Dipoles or Between Slots: With or Without Complex Conjugate? ,IEEE Transactions On Antennas And Propagation, Vol. 36, No. 10, October 1988
- [9] S . A. Schelkunoff, Theory of antennas of arbitrary size and shape, Proc. IRE, vol. 29, pp. 493-521, Sept. 1941.
- [10] E. C. Jordan and K. G. Balmain, Electromagnetic Waves and Radiating Systems, Englewood Cliffs, NJ, Prentice-Hall, 1968.
- [11] C. T. Tai, A study of the e.m.f. method, J. Appl. Phys., Vol. 20, pp. 717-723, July 1949.
- [12] Gray A. Thiele, Analysis of Yagi-Uda-Type Antennas, IEEE Transactions On Antennas And Propagation, Vol. AP-17, No. 1, January 1969.

- [13] Chen C., Cheng D., Optimum element lengths for Yagi-Uda arrays, IEEE Transactions on Antennas and Propagation , Volume: 23 , Issue: 1 , Jan 1975 Pages:8 - 15
- [14] Eric A. Jones and William T. Joines, Design of Yagi-Uda Antennas Using Genetic Algorithms, IEEE Transactions On Antennas And Propagation, Vol. 45, No. 9, September 1997.
- [15] Altshuler E.E., Linden D.S., Wire-antenna designs using genetic algorithms, Antennas and Propagation Magazine, IEEE , Volume: 39 , Issue: 2 , April 1997 Pages:33 - 43
- [16] Ramos R.M., Saldanha R.R., Takahashi R.H.C., Moreira F.J.S., The real-biased multiobjective genetic algorithm and its application to the design of wire antennas, IEEE Transactions On Magnetics, Vol. 39, No. 3, May 2003
- [17] Austin B.A., Wen-Chung Liu, An optimized shaped Yagi-Uda array using the genetic algorithm, IEE National Conference on Antennas and Propagation, 1999
- [18] Jones E.A., Joines, W.T.; Genetic design of linear antenna arrays, Antennas and Propagation Magazine, IEEE , Volume: 42 , Issue: 3 , June 2000 Pages:92 - 100
- [19] Correia D., Soares A.J.M., Terada M.A.B., Optimization of gain impedance and bandwidth in Yagi-Uda antennas using genetic algorithm, Microwave and Optoelectronics Conference, vol. 1, Aug. 1999
- [20] D. E. Goldberg, Genetic Algorithms, New York: Addison Wesley, 1989, ch.1-4.
- [21] C. A. Balanis, Antenna theory analysis and design, 2nd ed., New York: John Wiley and sons, 1996, ch.4.
- [22] Noriaki Kaneda, Yongxi Qian and Tatsuo Itoh, A Broad-Band Microstrip-to-Waveguide Transition Using Quasi-Yagi Antenna, IEEE Transactions On Microwave Theory And Techniques, Vol. 47, No. 12, December 1999
- [23] Phillip R. Grajek, Bernhard Schoenlinner and Gabriel M. Rebeiz, A 24-GHz High-Gain YagiUda Antenna Array, IEEE Transactions On Antennas And Propagation, Vol. 52, No. 5, May 2004
- [24] Edward B. and Rees D. , A broadband printed dipole with integrated balun, Microwave Journal, May 1987, pp. 339-344.
- [25] Chalmers M. Bulter, The equivalent Radius of a Narrow Conducting Strip, IEEE Transactions On Antennas And Propagation, Vol. Ap-30, No. 4, July 1982

APPENDIX A

In this appendix the near-field radiated electric field for a current distribution given in (1.9) will be derived.

Starting from the vector potential

$$A(x, y, z) = \frac{\mu}{4\pi} \int I_e(x', y', z') \frac{\exp(-jkR)}{R} dl' \quad (\text{A-1})$$

The magnetic field is calculated from A vector by

$$H = \frac{1}{\mu} \nabla \times A \quad (\text{A-2})$$

For this problem the currents is in the z direction so we have $A_x = A_y = 0$ and in polar coordinate we have

$$A_r = A_z \cos \theta, A_\theta = -A_z \sin \theta, A_\phi = 0 \quad (\text{A-3})$$

Using the symmetry of the problem(no variations in ϕ), (A.2) can be expanded in spherical coordinate and written in simplified form as

$$H = \widehat{a}_\phi \frac{1}{\mu r} \left[\frac{\partial}{\partial r} (r A_\theta) - \frac{\partial A_r}{\partial \theta} \right] \quad (\text{A-4})$$

Using (A.3) in (A.4) will give

$$H = -\widehat{a}_\phi \frac{1}{\mu} \left[\frac{\partial}{\partial r} (A_z) \right] \sin \theta \quad (\text{A-5})$$

Suppose the dipole lying along the z -axis in the center of coordinate system and we want to calculate the field at point $(0, y, z)$. In this case we will have

$$r^2 = y^2 + z^2, \frac{\partial r}{\partial y} = \frac{y}{r} \quad (\text{A-6})$$

Now using (A.6) in (A.5) and substituting for A vector with $I_e = I_0 \cos(\frac{\pi z'}{L})$ will give

$$H = -a_\phi \frac{I_0}{4\pi} \frac{\partial}{\partial y} \int_{-L/2}^{L/2} \frac{e^{-jkr}}{r} \cos \frac{\pi z'}{L} dz' \quad (\text{A-7})$$

and after applying the derivative and some simplification we will have

$$H = -a_\phi \frac{I_0}{4\pi y} \int_{-L/2}^{L/2} (r^2 - z^2) \left[\frac{-jke^{-jkr}}{r^2} - \frac{e^{-jkr}}{r^3} \right] \cos \frac{\pi z'}{L} dz' \quad (\text{A-8})$$

Electric field can now be calculated using

$$E = \frac{1}{j\omega\epsilon} \nabla \times H \quad (\text{A-9})$$

which will be simplified because of symmetry to

$$E_z = \frac{1}{j\omega\epsilon y} \frac{\partial}{\partial y} (yH_\phi) \quad (\text{A-10})$$

Using (A-8) in (A-10) with some simplification will give

$$E_z = \frac{1}{4\pi j\omega\epsilon} \int_{-L/2}^{L/2} \frac{e^{-jkr}}{r^5} [(1 + jkr)(2r^2 - 3b^2) - b^2k^2r^2] \cos \frac{\pi z'}{L} \quad (\text{A-11})$$

where

$$b^2 = r^2 - z^2 \quad (\text{A-12})$$

and b is the horizontal distance between the dipole and the point where the field is calculated.

The radiated near-field from equation (A-11) is plotted along a line in front of a dipole with the length of $\lambda/3$ in figure A.3 and in front of a dipole with the length of $2\lambda/3$ in figure A.4. The electric field is plotted for two kind of current distribution on the dipole. The solid line shows the electric field from a piece-wise sinusoidal current distribution given as $I_e = I_0 \sin[k(L/2 - |z'|)]$ and the dashed line shows the electric field radiated from a cosine current distribution given as $I_e = I_0 \cos(\frac{\pi z'}{L})$. The electric field are calculated in a line parallel to the wire with the distance of $\lambda/4$ from the wire. Figures A.1 and A.2 show the two current distribution for two different length of wires. It is assumed that $\lambda = 1$ in the plots and the amplitude of the current on the dipoles are in Ampere.

Note that in order to calculate the self impedance of a dipole, one has to set b equal to a (the radius of dipole) in (A.11) in order to calculate the generated field of the dipole on its surface.

APPENDIX B

In this appendix the far-field radiation pattern for an arbitrary length dipole with cosine current distribution is derived.

The argument starts by using equation (4-58a) from Balanis [21] and substituting (1.9) which will give us

$$E_{\theta} = j\eta \frac{kI_0 e^{-jkr}}{4\pi r} \sin \theta \int_{-L/2}^{L/2} \cos \frac{\pi z'}{L} e^{jkz' \cos \theta} dz' \quad (\text{B-1})$$

using

$$\cos \frac{\pi z'}{L} = \frac{e^{\frac{j\pi z'}{L}} + e^{-\frac{j\pi z'}{L}}}{2} \quad (\text{B-2})$$

and calculating the integral will give E_{θ} as

$$E_{\theta} = j\eta \frac{I_0 \exp(-jkr)}{2\pi r} \frac{\pi k}{L} \frac{\cos(\frac{kL}{2} \cos \theta)}{(\pi/L)^2 - k^2 \cos^2(\theta)} \sin \theta \quad (\text{B-3})$$

which will simplify to equation (B-4) as given by Balanis [21] eq.(4-62a) for $L = \lambda/2$.

$$E_{\theta} = j\eta \frac{I_0 \exp(-jkr)}{2\pi r} \frac{\cos(\frac{kL}{2} \cos \theta) - \cos(\frac{kL}{2})}{\sin \theta} \quad (\text{B-4})$$

APPENDIX C

The input file for NEC2 simulation is shown here for the 4-element Yagi in chapter one and the high gain Yagi explained in chapter 2. One important consideration in using NEC2 is a frequency correction that is needed to be done due to a different treatment of wavelength in two codes. In NEC2 the speed of light is considered to be $2.9975 \times 10^8 m/s$ where in the Matlab simulation speed of light is considered to be $3 \times 10^8 m/s$ and the frequency correction should be considered in the NEC2 input file to get the right results.

cm 4-element yagi

ce

gw3,5,0.1491,-.1707,0.0,0.1491,.1707,0.0,0.0025

gw4,5,0.405,-.166,0.0,0.405,.166,0.0,0.0025

gw48,5,0,-.1875,0,0,.1875,0,0.0025

gw49,5,-.1968,-.1802,0.0,-.1968,.1802,0.0,0.0025

gm,0,0,0.0,-90.0,0.0,0.0,0.0,0.0,0

ge

ek

fr0,1,0.0,0.0, 395.65,5.0

ex0,48,3,1,1.0,0.0,0.0

pt

ld

rp0,91,2,1501,0.0,0.0,2.0,90.0,0.0,0.0

cm high gain yagi

ce

gw3,5,0.122,-.172,0.0,0.122,.172,0.0,0.0025

gw4,5,0.319,-.169,0.0,0.319,.169,0.0,0.0025

gw5,5,0.525,-.162,0.0,0.525,.162,0.0,0.0025

gw6,5,0.652,-.139,0.0,0.652,.139,0.0,0.0025

gw7,5,0.751,-.159,0.0,0.751,.159,0.0,0.0025

gw8,5,0.951,-.119,0.0,0.951,.119,0.0,0.0025

gw9,5,1.047,-.158,0.0,1.047,.158,0.0,0.0025

gw10,5,1.338,-.151,0.0,1.338,.151,0.0,0.0025

gw11,5,1.470,-.147,0.0,1.470,.147,0.0,0.0025

gw12,5,1.698,-.154,0.0,1.698,.154,0.0,0.0025

gw13,5,1.945,-.148,0.0,1.945,.148,0.0,0.0025

gw14,5,2.104,-.151,0.0,2.104,.151,0.0,0.0025

gw15,5,2.327,-.154,0.0,2.327,.154,0.0,0.0025

gw16,5,2.554,-.148,0.0,2.554,.148,0.0,0.0025

gw17,5,2.850,-.154,0.0,2.850,.154,0.0,0.0025

gw18,5,3.144,-.154,0.0,3.144,.154,0.0,0.0025

gw19,5,3.409,-.145,0.0,3.409,.145,0.0,0.0025

gw20,5,3.569,-.145,0.0,3.569,.145,0.0,0.0025

gw21,5,3.867,-.148,0.0,3.867,.148,0.0,0.0025
gw22,5,4.078,-.118,0.0,4.078,.118,0.0,0.0025
gw23,5,4.270,-.147,0.0,4.270,.147,0.0,0.0025
gw24,5,4.543,-.156,0.0,4.543,.156,0.0,0.0025
gw25,5,4.837,-.127,0.0,4.837,.127,0.0,0.0025
gw26,5,5.072,-.142,0.0,5.072,.142,0.0,0.0025
gw27,5,5.330,-.148,0.0,5.330,.148,0.0,0.0025
gw28,5,5.574,-.149,0.0,5.574,.149,0.0,0.0025
gw29,5,5.775,-.156,0.0,5.775,.156,0.0,0.0025
gw30,5,6.052,-.139,0.0,6.052,.139,0.0,0.0025
gw31,5,6.331,-.160,0.0,6.331,.160,0.0,0.0025
gw48,5,0,-.1875,0,0,.1875,0,0,0.0025
gw49,5,-.193,-.188,0.0,-.193,.188,0.0,0.0025
gm,0,0,0.0,-90.0,0.0,0.0,0.0,0.0,0
ge
ek
fr0,1,0.0,0.0, 395.65,5.0
ex0,48,3,1,1.0,0.0,0.0
rp0,91,2,1501,0.0,0.0,2.0,90.0,0.0,0.0

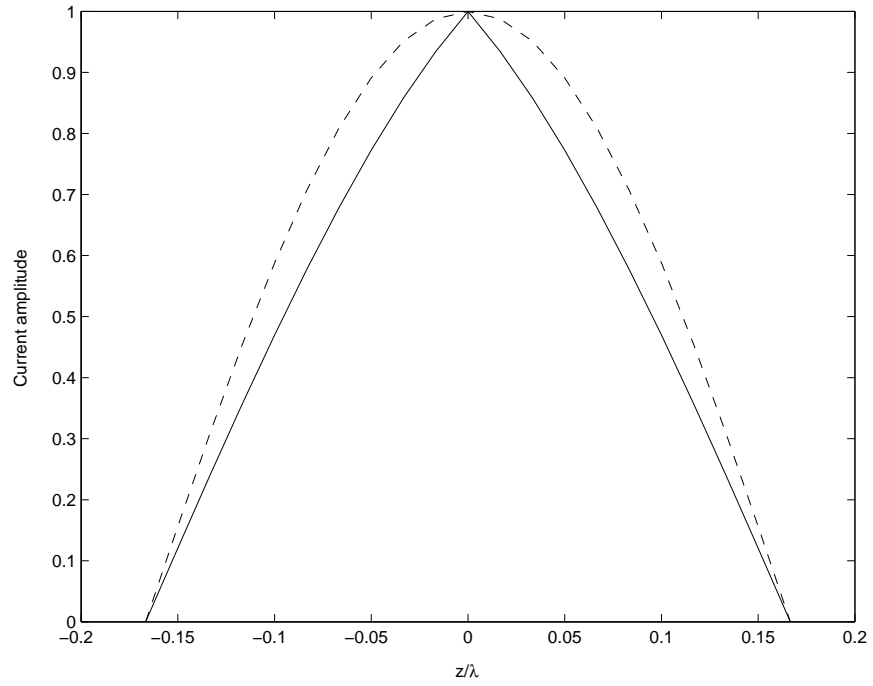


Figure A-1: Plot of the current distribution of a $\lambda/3$ dipole. Solid line: piecewise sinusoidal current, Dashed line: cosine current

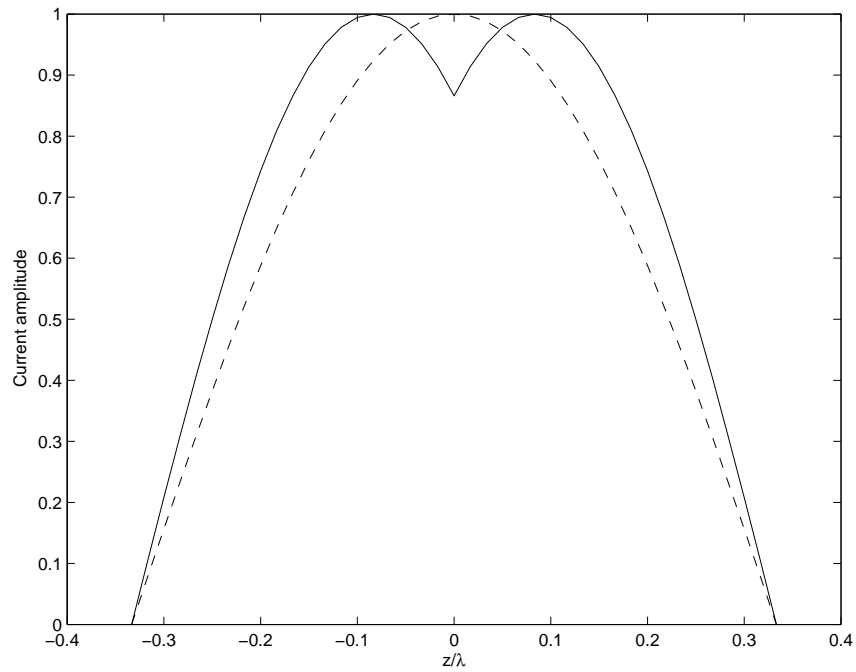


Figure A-2: Plot of the current distribution of a $2\lambda/3$ dipole. Solid line: piecewise sinusoidal current, Dashed line: cosine current

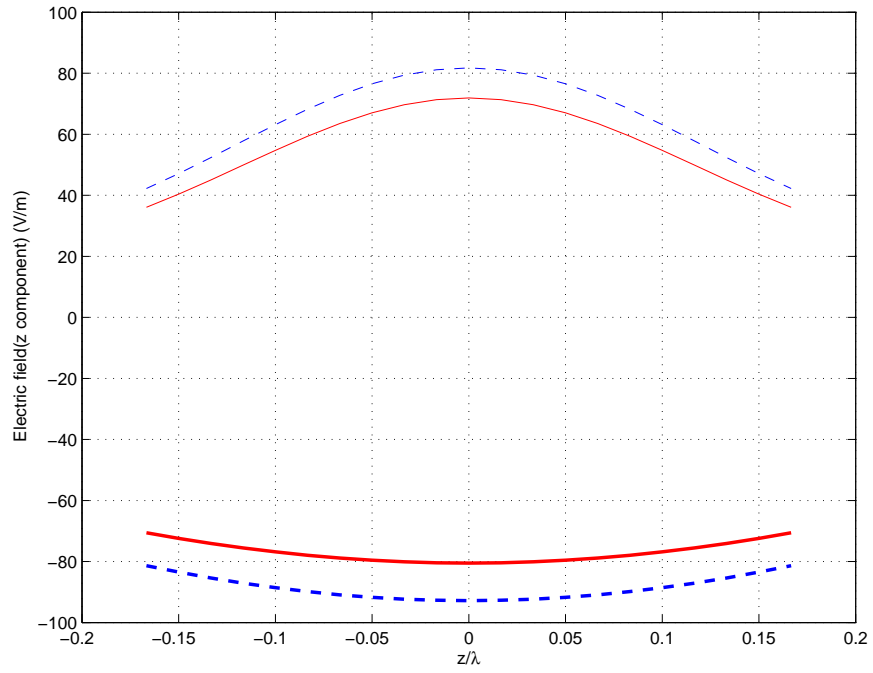


Figure A-3: $L = \lambda/3$: Plot of the electric field along a parallel line, $\lambda/4$ away from the dipole. Solid line: piece-wise sinusoidal current, Dashed line: cosine current, Thick line: real part of the field, Thin line: imaginary part of the field

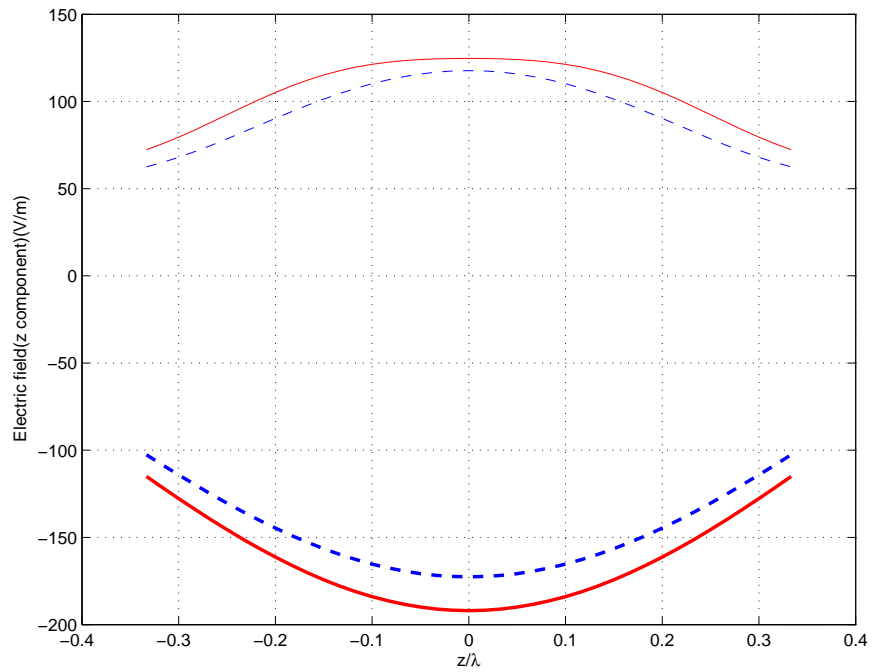


Figure A-4: $L = 2\lambda/3$: Plot of the electric field along a parallel line, $\lambda/4$ away from the dipole. Solid line: piece-wise sinusoidal current, Dashed line: cosine current, Thick line: real part of the field, Thin line: imaginary part of the field